Biological activity *In vitro*, absorption, BBB penetration and toxicity of nanoformulation of BT44, a RET agonist with disease-modifying potential for the treatment of neurodegeneration

Malik Salman Haider[1,‡,*], Arun Kumar Mahato[2,‡], Anastasiia Kotliarova[2], Stefan Forster[1], Bettina Böttcher[3], Philipp Stahlhut[4], Yulia Sidorova[2,*‡], Robert Luxenhofer[1,5‡]

[1]*Functional Polymer Materials, Chair for Advanced Materials Synthesis, Institute for Functional Materials and Biofabrication, Department of Chemistry and Pharmacy, Julius-Maximilians-University Würzburg, Röntgenring 11, 97070 Würzburg, Germany*

[2]*Laboratory of Molecular Neuroscience, Institute of Biotechnology, HiLIFE, University of Helsinki, 00014, Helsinki, Finland*

[3]*Biocenter and Rudolf Virchow Centre, Julius-Maximilians-University Würzburg, Haus D15, Josef-Schneider-Str. 2, 97080 Würzburg, Germany*

[4]*Department of Functional Materials in Medicine and Dentistry, Institute of Functional Materials and Biofabrication and Bavarian Polymer Institute, Julius-Maximilians-University Würzburg, Pleicherwall 2, 97070 Würzburg, Germany*

[5]*Soft Matter Chemistry, Department of Chemistry, and Helsinki Institute of Sustainability Science, Faculty of Science, University of Helsinki, PB 55, 00014 Helsinki, Finland*

Keywords: Receptor tyrosine kinase RET, RET agonist, glial cell line-derived neurotrophic factor (GDNF), neurodegeneration, blood brain barrier, solubility enhancement, drug delivery, amphiphilic block copolymer, poly(2-oxazoline), nanomedicine

‡ contributed equally

*Correspondence to: malik.haider@uni-wuerzburg.de and yulia.sidorova@helsinki.fi

Abstract

BT44 is a novel, second generation glial cell line-derived neurotropic factor (GDNF) mimetic, with improved biological activity and a lead compound for the treatment of neurodegenerative disorders. Like many other small molecules, it suffers from intrinsic poor aqueous solubility, posing significant hurdles at various levels for its preclinical development and clinical translation. Herein, we report a novel poly(2-oxazoline)s (POx) based BT44 micellar nanoformulation with ultra-high drug loading capacity of 47 wt.%. The BT44 nanoformulations were comprehensively characterized by ^{1}H-NMR spectroscopy, differential scanning calorimetry (DSC), powder X-ray diffraction (XRD), dynamic light scattering (DLS) and cryo-transmission/scanning electron microscopy (cryo-TEM/SEM). The DSC, XRD and redispersion studies collectively confirmed that the BT44 formulation can be stored as a lyophilized powder and can be redispersed when needed. The DLS further suggested that the redispersed formulation is suitable for parenteral administration (D_h ≈ 70nm). The cryo-TEM analysis revealed the presences of worm like structures. The BT44 formulation retains biological activity in immortalized cells and in cultured dopamine neurons. The micellar formulation of BT44 exhibited improved absorption and blood-brain barrier (BBB) penetration and produced no acute toxic effects in mice. In conclusion, herein, we have developed an ultra-high BT44 loaded aqueous injectable nanoformulation, which can be used to pave way for its preclinical and clinical development for the management of neurodegenerative disorders.

Introduction

In the past decades, drug discovery has seen significant advancements in technological innovation resulting in development of large number of potential candidates as drug molecules. However, according to some estimate, 90% of the drugs in the development pipeline and 40% of the drugs in the market are highly hydrophobic [1]. Unfortunately, poor intrinsic aqueous solubility is a common factor in both synthetic and naturally occurring pharmacophores [2], posing a significant risk for varied oral absorption and require special vehicle for injectable applications. The aqueous solubility plays a

pivotal role in the overall product design to attain higher bioavailability and therapeutic concentration at the site of interest.

Aging population bring new challenges and demands to the society in the context of drug development. Elderly people often suffer from co-morbidities that require diverse pharmacological management. In particular, currently incurable neurodegenerative disorders such as Parkinson's disease (PD), retinal degeneration, amyotrophic lateral sclerosis and neuropathic pain affect increasing number of patients in the modern society. These disorders are caused by the death of various neuronal populations in the body and are currently incurable [3-5]. The potential disease-modifying treatments can be developed on the basis of neurotrophic factors, secreted proteins which function as the survival and maintenance factors for both developing and mature neurons [6].

Glial cell line-derived neurotrophic factors (GDNF) is the most promising for the treatment of PD. GDNF first binds to glycosylphosphatidylinositol-anchored co-receptor GDNF family receptor α and then form a complex with Rearranged during transfection (RET) receptor tyrosine kinase resulting in activation of RET and RET downstream signalling cascades necessary for the cellular processes like migration, proliferation, differentiation and metabolism [6]. However, GDNF lacks drug-like properties making its clinical translation difficult. We have designed and developed series of RET agonists that can bind and activate RET receptor similarly to GDNF [6-8]. Among them, BT44 is a second generation compound that alleviated neuropathic pain in both surgery-based and diabetes-induced models of neuropathic pain [9]. Further, BT44 also protected cultured dopamine neurons from neurotoxic damage. It also alleviated motor symptoms and protected dopaminergic fibers in the striatum of 6-hydroxydopamine (6-OHDA) model of PD [10]. Therefore, it is a promising lead compound for the treatment of neurodegenerative disorders and neuropathic pain [9, 10]. However, BT44 suffers from intrinsic poor aqueous solubility like many other hydrophobic drugs, posing significant hurdles at various levels for its preclinical development and clinical translation.

Various methods such as the preparation of salts forms, drug complexes, use of co-solvents [11], drug emulsification, micro-/nanonization, crystal engineering, solid dispersion [12, 13] and

nanotechnological approaches are used to enhance the (apparent) aqueous solubility of such molecules. Among all, the nanocarrier approach is a rapidly emerging tool to address such issues [14, 15]. A plethora of studies showed the utilization of nanoparticles, nanospheres, nanocapsules, nanosuspension/-emulsion and micelles for drug delivery applications mainly in the context of solubility enhancement [16, 17].

Besides others, over the last thirty years, the polymer micelles (PMs) evolved as promising hydrophobic drug solubilisation and/or delivery vehicle [18-20]. They are self-assembled colloidal particles made up of block copolymers comprising hydrophilic and hydrophobic domains [21]. It is commonly believed that the hydrophobic core is responsible for drug encapsulation and the hydrophilic shell interacts with solvent molecules (representing core-shell morphology) providing colloidal stability [22, 23]. Depending on the nature of the hydrophilic domain, cargo and employed (cargo) load, it is becoming more evident that at certain threshold drug concentration, the hydrophilic domain also starts to interact [24-29] with the cargo, indicative of much complex morphologies [30-32]. To date, many polymeric micellar formulations underwent preclinical and clinical trials presenting improved pharmacological activity with lower systemic toxicity [20, 33-35], but successful translation into clinics have been few. Like other excipients used for formulation development, amphiphilic block copolymers used as vehicles must also be pharmacologically inert and clinically safe [36].

In the past decades, polymers of cyclic imino ethers [37], particularly poly(2-oxazoline)s (POx) and poly(2-oxazines)s (POzi) have seen significant attention because of their potential in tissue engineering [38-40], drug delivery [35, 41-48] and 3D (bio) printing [49-51]. Based on a highly variable molecular toolbox, fine tuning of the amphiphilic character in AB diblock, ABA triblock or more complex architectures [52] is readily achieved (where A and B are hydrophilic and hydrophobic domains, respectively) [50, 53-55]. In particular, ABA triblock copolymers featuring poly(2-methyl-2-oxazoline) (pMeOx) as hydrophilic A blocks and moderately hydrophobic poly(2-*n*-butyl-2-oxazoline) (pBuOx), poly(2-*n*-butyl-2-oxazine) (pBuOzi) or poly(2-*n*-propyl-2-oxazoline) (pPrOx) show very interesting properties such as ultra-high drug loading, excellent cytocompatibility and are very well tolerated

upon *in vivo* administration [42, 49, 56, 57]. More importantly, they allow significant therapeutic improvements as demonstrated for several drugs and drug combinations [35, 58-60]. Accordingly, here we prepared and investigated a nanoformulation of BT44, a compound which has poor intrinsic aqueous solubility, using POx based ABA triblock copolymers. To the best of our knowledge, this represents the first example of a micellar BT44 nanoformulation with a detailed physicochemical characterization which retains biological activity, demonstrates improved absorption and better blood-brain barrier (BBB) penetration compared to the non-formulated drug.

Materials and Methods

All substances for the synthesis of polymers were purchased from *Sigma-Aldrich* (Steinheim, Germany) or *Acros* (Geel, Belgium) and were used as received unless otherwise stated. The monomers used in this study are 2-*n*-propyl-2-oxazoline (PrOx), 2-*n*-butyl-2-oxazoline (BuOx) and 2-*n*-pentyl-2-oxazoline (PentOx). The monomer PentOx was synthesized for this study according following a modified procedure of Witte and Seeliger [61] as reported recently [53, 62]. All the other substances used for polymerization i.e. methyl trifluoromethylsulfonate (MeOTf), 2-methyl-2-oxazoline (MeOx) and solvents for polymer synthesis were refluxed over CaH_2, while benzonitrile (PhCN) was refluxed over P_2O_5 and distilled under argon. Deuterated solvents for NMR analysis were purchased from *Deutero GmbH* (Kastellaun, Germany).

Monomer synthesis

Hexanenitrile (1 equiv.), 1.2 equiv. of ethanolamine and 0.025 equiv. of zinc acetate dihydrate were added to a nitrogen flushed flask and heated to 130 °C (SI; synthesis 1). The reaction was kept under reflux (for 4 days) until the reaction mixture turned dark brown. Reaction progress was controlled by ^{1}H-NMR-spectroscopy. The raw product was dissolved in chloroform (30 mL) and washed with deionized (DI) water (60 mL, 3 times). The organic phase was collected and dried with sodium sulfate, filtered and concentrated under vacuum. The residue was mixed with calcium hydride and distilled under vacuum. If necessary, distillation was repeated and the product was stored under argon atmosphere. Further synthesis details can be found in the supporting information.

Polymer synthesis

The polymerizations and work-up procedures for A-pPrOx-A and A-pBuOx-A triblock copolymers were previously reported [53, 62-64]. The synthesis of A-pPentOx-A triblock copolymer was performed as follows (for details, see supporting information; synthesis 2): the initiator, MeOTf was added to a dried and argon flushed flask followed by PhCN addition. Further, MeOx was added, the reaction mixture was heated to 110°C and incubated at that temperature for approximately 4 hours. Reaction progress was controlled by ^{1}H-NMR-spectroscopy. After complete consumption of MeOx, the mixture was cooled to room temperature and the monomer for the second block i.e. PentOx was added. The reaction mixture was heated to 110°C and kept on stirring overnight. The procedure was repeated for the third block (MeOx) and after confirmation of full monomer consumption, termination was carried out by addition of 5 eq. of 1 M NaOH aqueous solution and the mixture was stirred at 50°C for 4 hours. PhCN was removed under reduced pressure. The highly viscous residues were dissolved in DI water, transferred into a dialysis bag (molecular weight cut-off (MWCO) 1 kDa, cellulose acetate), and dialyzed against DI water for 24 h. The solution was recovered from the bag and lyophilized. The product was obtained as white powder (Yield = 92%).

Lead compound; BT44

BT stands for Baltic Technology, a company, which was originally involved into the discovery of this scaffold. The chemical name for the BT44 is ((4-5-((3,4-dihydroisoquinolin-2(1H)-yl) sulfonyl)-2-methoxyphenyl) piperazin-1-yl (4-fluoro-2 (trifluoromethyl)phenyl) methanone, MW: 577.59. The compound was synthesized by EvoBlocks (Hungary, Cat# EBR-10719615). The purity of BT44 was determined by HPLC (97.3%.) and further the chemical structure was verified by NMR spectroscopy. The experiments were performed on a Bruker Avance III HD NMR spectrometer operated at 1H frequency of 850.4 MHz equipped with a cryogenic probe head by NMR facility at the Institute of Biotechnology, University of Helsinki, Finland.

Methods

Nuclear Magnetic Resonance Spectroscopy (NMR)

NMR spectra for this study were recorded on a Fourier 300 (300.12 MHz), *Bruker Biospin* (Rheinstetten, Germany) at 298 K. The spectra were calibrated to the signal of residual protonated solvent ($CDCl_3$ at 7.26 ppm, D_2O at 4.79ppm) and analyzed using MestReNova software (version 6.0.2-5475).

Dialysis

Dialysis was performed using Spectra/Por membranes with a MWCO of 1 kDa (material: cellulose acetate) obtained from *neoLab* (Heidelberg, Germany). DI water was renewed after 1, 4, 12 and 24 h and the resulting formulation was lyophilized.

Gel Permeation Chromatography (GPC)

Gel permeation chromatography (GPC) was performed on SECurity GPC Agilent 1260 Infinity System (*Polymer Standard Service* (Mainz, Germany) with HFIP containing 3 g/L potassium trifluoroacetate; precolumn: 50 x 8 mm PSS PFG linear M; 2 columns: 300 x 8 mm PSS PFG linear M (particle size 7 µm; pore size 0.1 – 1,000 kDa). The columns were kept at 40°C and flow rate was 0.7 ml/min. Prior to each measurement, samples were filtered through 0.2 µm Teflon (PTFE) filters, *Roth* (Karlsruhe, Germany). Conventional calibration was performed using poly(ethylene glycol) standards (0.1 – 1,000 kg/mol) and data was processed with Win-GPC software and further plotted in OriginPro 2015 Sr2 (version b9.2.272) software.

Polymer-drug compatibility by solubility parameters

The extent of compatibility between BT44 and the hydrophobic block of the A-B-A triblock copolymers was estimated by using the Hildebrand-Scatchard equation [65].

$$\chi_{drug-polymer} = (\delta_{drug} - \delta_{polymer})^2 \frac{V}{RT} \quad (1)$$

Where $\chi_{drug\text{-}polymer}$ (χ_{dp}) represents the Flory-Huggins interaction parameter, δ_{drug} and $\delta_{polymer}$ are the solubility parameters for the drug (BT44) and polymer, respectively. V is the molar volume of BT44 calculated by Fedor's method [66], R is the gas constant and T is the temperature in K. The δ_{drug} and $\delta_{polymer}$ were calculated by following equations:

$$\delta_{drug}^2 = \delta_d^2 + \delta_p^2 + \delta_h^2 \quad (2)$$

$$\delta_{polymer}^2 = \delta_d^2 + \delta_p^2 + \delta_h^2 \quad (3)$$

The δ_{drug} and $\delta_{polymer}$ are representing the total solubility parameters (δ_{total}) for drug and polymer, respectively. The δ_{total} is the sum of dispersion (δ_d), polar (δ_p) and hydrogen bonding contributions (δ_h). The δ_d, δ_p and δ_h were further calculated by Hoftyzer and Van Krevelen's additive group contribution method by using the following equations:

$$\delta_d = \frac{\sum Fdi}{V} \qquad \delta_p = \frac{(\Sigma F_{pi}^2)^{1/2}}{V} \qquad \delta_h = \left(\Sigma \frac{E_{hi}}{V}\right)^{1/2} \qquad (4, 5, 6)$$

Where F_{di}, F_{pi} and E_{hi} are the molar dispersion, polar attraction constant and hydrogen bonding energy, respectively. Each structural group in the molecule contribute towards the F_{di}, F_{pi} and E_{hi}, the values were obtained from literature [67].

Drug formulation

Drug loaded polymer micelles were prepared using the thin film hydration method. Polymer (10 or 100 g/L) and BT44 (15 g/L) stock solutions in EtOH were mixed in desired ratios. After complete removal of the solvent at 50°C under a mild stream of argon, to remove the traces of ethanol (if any), the films were further dried *in vacuo* (≤ 0.2 mbar) for at least 30 minutes. Subsequently, preheated (37°C) DI water was added to obtain the desired final polymer (10 or 100 g/L) and BT44 concentrations. To ensure complete solubilisation, the solutions were shaken at 55°C for 15 to 30 min at 1250 rpm with a Thermomixer comfort (*Eppendorf AG,* Hamburg, Germany). Non-solubilized drug was removed by centrifugation for 5 min at 10,000 rpm with a 3-Speed micro centrifuge, (*neoLab,* Heidelberg, Germany). Solubilisation experiments were performed in 3 individually prepared samples and results are presented as mean ± standard deviation (SD).

High performance liquid chromatography (HPLC)

HPLC analysis was carried out on a LC-20A Prominence HPLC (*Shimadzu,* Duisburg, Germany) equipped with a system controller CBM-20A, a solvent delivery unit LC-20 AT (double plunger), an on-line degassing unit DGU-20A, an auto-sampler SIL-20AC, a photo diode array detector SPD-M20A. As stationary phase, a ZORBAX Eclipse Plus (*Agilent,* Santa Clara, CA, USA) C18 column (4.6 x 100 mm; 3.5 µm) was used. Quantification of BT44 was performed with a stepwise gradient using acetonitrile (ACN) and water with 0.05% TFA. Within the first 10 min, the ratio of H_2O/ACN was gradually changed from

60/40 (v/v) to 40/60 (v/v). Within 10 seconds, the solvent was abruptly changed to 20/80 (v/v) and kept constant for 2 min, followed by sudden change back to 60/40 (v/v). This ratio was kept for next 8 min. Each HPLC measurement took 18 minutes with flow rate of 1 mL/min. Detection was performed at 230 nm and the retention time of BT44 was 12.6 min.

Loading capacity and loading efficiency (LC & LE)

The following equations were used to calculate the loading capacity (LC) and loading efficiency (LE) of the BT44 formulations:

$$LC = \frac{m_{drug}}{m_{drug} + m_{excipient}} * 100\%$$

$$LE = \frac{m_{drug}}{m_{drug,added}} * 100\%$$

where m_{drug} and $m_{excipient}$ are the weight amounts of the solubilized drug and polymer excipient in solution and $m_{drug,added}$ is the weight amount of the drug initially added to the dispersion. No loss of polymer during micelles preparation was assumed.

Stability studies

For stability studies, all the freshly prepared BT44 formulations were stored at ambient conditions (≈ 25°C) under the exclusion of light. The samples were collected at day 0, 1, 5, and 15. Before the determination of the drug loading by HPLC, all samples were centrifuged for 5 min at 10.000 rpm with a 3-Speed micro centrifuge (*neoLab,* Heidelberg, Germany) to remove any aggregates or agglomerates. All the formulations and stability experiments were performed with 3 individually prepared samples and results are presented as means ± SD, quantification was performed as described in HPLC section.

Redispersion studies

The freshly prepared formulations were frozen in liquid nitrogen and subjected to 24 h lyophilisation to get the BT44 formulation as dried powder for redispersion studies. The lyophilized formulations were redispersed in normal saline (0.9% NaCl) and cell culture media (Dulbecco's modified eagle

medium, DMEM). After the addition of solvent of interest, the formulations were shaken at 1250 rpm with a Thermomixer comfort (*Eppendorf AG,* Hamburg, Germany) at room temperature for 5 minutes followed by HPLC analysis as stated in HPLC section.

Differential scanning calorimetry (DSC)

DSC was performed on DSC 204 F1 Phoenix equipped with a CC200 F1 Controller, (*NETZSCH,* Selb, Germany). The dynamic scans were recorded in nitrogen atmosphere with a heating rate of 10K/min (0°C – 200°C). For DSC studies samples were placed into flat-bottom aluminum pans with pierced lids. The aqueous BT44 formulation was lyophilized to obtain the dry powdered formulation prior to DSC measurements. The DSC of pure polymer and pristine BT44 was also performed. The data was further analysed in thermoanalysis software and plotted in OriginPro 2015 Sr2 (version b9.2.272) software.

X-Ray diffraction (XRD)

Powder X-ray diffraction (XRD) of the lyophilized BT44 formulation was performed on X-ray diffractometer D8 Davinci Design (Bruker AXS). The setup is equipped with radiation source of Cu-Kα and the detector is linear position sensitive detector (PSD). Measurement were done at 0.02° steps each step lasting 1s in transmission mode at 40 kV voltage and 40 mA current and 2Θ angle ranging from 5° to 40° were used. The XRD of plain polymer and pristine BT44 was also performed under same set of conditions. The data was further analysed and plotted in OriginPro 2015 Sr2 (version b9.2.272) software.

Dynamic light scattering (DLS)

Dynamic light scattering were measured using a Zetasizer Nano ZSP from Malvern (at single angle of 173°), (Malvern Instruments, Worcestershire, UK) in disposable cuvettes (UV cuvettes semi micro, BRAND GmbH, Wertheim, Germany) at ambient temperature (≈ 25 °C). Plain polymer and various BT44 formulation were measured after filtration using 0.45 µm PVDF syringe filter (*Rotilabo*, Karlsruhe). The measurements were recorded as average of three test runs (each with 12 sub-

measurements) for one individually prepared sample. Data was analysed by using zetasizer software 7.11 and plotted in OriginPro 2015 Sr2 (version b9.2.272) software.

Cryogenic transmission electron microscopy (cryo-TEM)

The freshly prepared plain polymer solutions with concentration of 10 and 25 g/L (as free flowing liquid solution) and redispersed polymer/BT44 formulation at 10/2 g/L feed (n=1) were subjected to cryo-TEM studies. For sample preparation, copper grids coated with holey carbon support film (quantifoil, 400 mesh, R1/2) were glow-discharged in air for 1.5 min in a plasma cleaner (Harrick PDC-002). Afterwards, 5 µl of each solution was applied on the grids and plunge-frozen in liquid ethane with a Vitrobot IV (FEI Company, Hilsboro, USA). The humidity in the chamber was set to 100% and the temperature was kept at 25 °C. Following settings were further employed i.e. wait time 0 sec, drain time 0 sec, blot time 5 sec, blot force -5. Samples were imaged on a FEI Tecnai T12 Spirit transmission electron microscope (FEI Company, Hilsboro, USA) equipped with a LaB6 emitter at an acceleration voltage of 120 kV and a temperature of -180 °C. Images were recorded with an Eagle CCD camera (FEI Company, Hilsboro, USA) in low-dose mode with a total dose of 30 e/Å2 and a nominal under focus of -3 µm with serial EM [68]. The images were further processed in ImageJ software (1.46 r, revised edition).

Cryogenic scanning electron microscopy (cryo-SEM)

The higher plain polymer concentrations i.e. 50 and 100 g/L (as free flowing liquid solution) were visualized with cryo-SEM. Samples were rapidly frozen in slushed nitrogen at −210 °C after placing them between aluminum plates (d = 3 mm) with a 2 mm notch for sample fixation. All the following transfer steps were performed at −140 °C with an EM VCT100 cryo-shuttle (Leica Microsystems). To generate a freshly fractured polymer surface, one of the aluminum plates was knocked off and freeze etched for 15 min at −85 °C under high vacuum (<1×10^{-3} mbar) in a Sputter Coater machine (ACE 400, Leica Microsystems). Afterward, samples were sputtered with 3 nm platinum and transferred to the SEM chamber (Crossbeam 340, Zeiss). Images of the polymer surface morphology were taken at −140

°C using an acceleration voltage of 8 kV. The images were further processed in ImageJ software (1.46 r, revised edition).

Cytocompatibility studies of the polymer excipient

The cytocompatibility studies of the plain polymer were carried out on MG87 RET cells. The cell viability was examined using Alamar blue assay as described previously (Ardashov et al., 2019). MG87 RET cells were cultured overnight in 96 well plate (OptiPlate 96 F HB, Wallac). Various concentration of polymer (1, 5, 10, 50 g/L) dissolved in DMEM and 15 mM HEPES were applied to the cells. At 72-hour post-treatment, Alamar blue was dissolved in the cell culture media in the ratio 1:10 and applied to the cultured cells. The fluorescence was measured using Victor plate reader at an excitation wavelength at 540 and an emission wavelength at 590 nm nm after 2-hour incubation with Alamar blue. . The experiment was repeated 3 times independently.

RET phosphorylation assay

RET phosphorylation assay in response to BT44 was carried out in MG87 RET cells transfected with hGFRα1 and green fluorescent protein (GFP)-expressing plasmids as described previously (Leppänen et al., 2004; Sidorova et al., 2017). In short, MG87 RET cells were cultured in 6 well plates in DMEM, 10% FBS, 100 µg/ml normocin one day prior to the experiment. Subsequently, the cells were transfected with 4 µg/well of GFRα1- and GFP-expressing plasmid using Lipofectamine 2000 (Invitrogen) as described by the manufacturer. The cells were starved (starvation media: serum-free DMEM, 15 mM HEPES, pH 7.2) for 4 h and stimulated for 15 minutes with 0.64 mg/ml of polymer (represents same amount of polymer in formulation), 100 µM BT44 nanoformulation, 100 µM BT44 and 6.6 nM GDNF (PeproTech, Ltd) dissolved in starvation media. Then the cells were washed once with ice-cold PBS containing 1 mM Na_3VO_4 and lysed with RIPA-modified buffer (50 mM Tris-HCl, pH 7.4, 150 mM NaCl, 1 mM EDTA, 1% NP-40, 1% TX-100, 10% glycerol, EDTA-free protease inhibitor cocktail (Roche, Switzerland), 1 mM Na_3VO_4, 6 mM sodium deoxycholate, 1 mM PMSF) on ice. The supernatant obtained after centrifugation was used to immunoprecipitate RET with RET antibody (2

µg/ml, R&D, Cat# AF1485) bound to magnetic beads coated with protein G (Dynabeads Protein G, Life Technologies, USA). The precipitated immunocomplexes were resolved on SDS–PAGE, transferred to nitrocellulose membranes and probed with anti-phosphotyrosine antibodies (1:1500, clone 4G10, Merck Millipore, Germany, Cat# 05-321). Stained bands were visualized with enhanced chemiluminescence (ECL) reagent (Pierce) using LAS3000 imaging software. To ensure equal loading, membranes were stripped and re-stained with anti-RET C-20 antibody (1:500, R&D, Cat# AF1485).

Cell-based ^{125}I-GDNF-displacement assay

The cell-based **^{125}I-GDNF-displacement** assay was carried in HEK293 cells. The cells were cultured in DMEM, 10% FBS, 100 µg/ml normocin overnight and then transfected with GFRα1 or GFRα1 and RET using Lipofectamine 2000 (Invitrogen), as described by the manufacturer. Next day, the cells were incubated for 1 hour on ice in the presence of BT44 formulation in concentrations ranging from 0 to 50 pM. Afterwards 50 pM of iodinated GDNF was added and the cells were incubated for 1 hour on ice with **^{125}I-GDNF** and nanoformulated-BT44. Subsequently, cells were washed with PBS for four times and lysed with 1 M NaOH, lysates were collected into the scintillation vials and counted using Perkin Elmer Wallac Wizard 1470-020 Gamma Counter. The data for GFRα1-transfected cells were collected in 2 independent experiments and for GFRα1/RET-transfected cells in 4 independent experiments. The binding data were analyzed by nonlinear regression analysis using GraphPad Prism 8.4.2 software to determine the IC_{50} values. Experiments with non-formulated BT44 were not conducted because of insufficient solubility of the compound in assay media.

Binding assay using microscale Thermophoresis

The molecular interaction between nanoformulated BT44 and the receptors was studied using microscale thermophoresis (MST). Non-formulated BT44 was not studied in this assays due to insufficient solubility. All the experiments were performed using Monolith NT.115 instrument (NanoTemper Technologies GmbH, Germany). Recombinant human GFRα1 or RET extracellular domain were labelled through His-tag using Monolith His-Tag Labeling Kit RED-tris-NTA (NanoTemper Technologies GmbH; MO-L008). The His-labelled GFRα1 or RET was used at 20 nM. The starting

concentration of nanoformulated BT44 (ligand) was 10 µM which was chosen based on the result obtained from cell based experiment. All the measurements were performed using premium coated capillaries (NanoTemper Technologies GmbH; MO-K025) in a buffer containing 20 mM of HEPES, 150 mM NaCl, 186 µM $CaCl_2$ and 0.05% Tween-20. The measurements of the interaction between formulation and the receptors were carried using red LED source, power set at 100% and medium MST power at 25 °C. The data were obtained from three independent experiments and were analyzed using MO. Affinity Analysis software v2.3 and dissociation constant (Kd) was calculated .

Neuroprotective effect of nanoformulated BT44 in primary dopamine neurons culture

The neuroprotective effect of plolymer, nanoformulated BT44 and pristine BT44 dissolved in Dimethyl sulfoxide (DMSO)was studied in 1-methyl-4-phenylpyridinium (MPP+)-challenged dopamine neurons as described previously (Ardashov et al., 2019; Mahato et al., 2020; Renko et al., 2021). Mid brain dopamine neurons were isolated from E13.5 embryos of NMRI mice and cultured for 5 days in dopamine neuron culture medium [(Dulbecco's MEM/Nut mix F12 (Invitrogen/Gibco, Cat# 21331-020), 1xN_2 serum supplement (Invitrogen/Gibco, Cat# 17502-048), 33 mM D-glucose (Sigma-Aldrich, Germany, Cat# G-8769), 0.5 mM L-glutamine (Invitrogen/Gibco, Cat# 25030-032), and 100 µg/ml Primocin (InvivoGen, USA, Cat# ant-pm-2)]. On the day 6, polymer (6.4 µg/ml), nanoformulated BT44 (100nM) or DMSO BT44 (100 nM) and GDNF (3.3 nM) was added to the cells for the period of 48 hours. Afterwards, the media was removed and cells were fixed with 4% paraformaldehyde (PFA) for 20 minutes, washed with PBS and permeabilized with 0.2 % TritonX-100 in PBS. Further, cells were blocked with 5% horse serum for one hour and then incubated with mouse anti-TH antibody (1:2000, Merck Millipore, Cat# MAB318) overnight at 4 °C. Subsequently, cells were washed and incubated with Alexa Fluor™ 647 conjugated donkey anti-mouse secondary antibody (1:500, Thermo Fisher Scientific, USA, Cat# A-31571) and 0.2 µg/ml DAPI (4', 6-diamidino-2-phenylindole) for 1 hour at room temperature. Finally, cells were imaged by ImageXpress Nano Automated Imaging System (Molecular Devices) at 10× magnification. The images were analyzed using CellProfiler image analysis software to

calculate the number of tyrosine hydroxylase (TH)-positive cells. Resulting data were subjected to statistical analysis in GraphPad Prism software

In vivo studies

Experimental animals

The animals (mice) used in the experiments were housed under 12 hours light–dark cycle with food and water available ad libitum. The experiments were carried out in accordance with 3R principle, European Community guidelines for the use of experimental animals and approved by the National Animal Experiment Board of Finland (license numbers ESAVI/7551/04.10.07/2013 and ESAVI/198/04.10.07/2014) for experiments with living animals. Animals for acute toxicity studies were leftover animals from breeding experiments (Mouse line: C57BL/6JRccHsd and B6C3-Tg(HD82Gln)81Gschi/J). Both males and females mice (age = 4-5 months) were used for the experiments. The use of animal for primary neuronal culture was approved by Laboratory Animal Centre of the University of Helsinki (license number KEK15-022). The primary dopamine culture was prepared from E13.5 embryos of NMR1 mice.

In vivo assessment of acute toxicity of BT44 in propylene glycol or as aqueous POx formulation

The acute toxicity in mice was studied in experiment with cross-over design. Mice (n = 24) were randomly divided into 8 groups (3 mice in each). In the first period of experiment mice from group 1 to 8 were subcutaneously injected with normal saline, propylene glycol (PG), plain polymer (355 and 586 mg/kg), nanoformulated BT44 at 25 and 50 mg/kg, and BT44 dissolved in PG (25 and 50 mg/kg), respectively. The injection volume was 10 ml/kg. The amount of polymer in the nanoformulated BT44 is same as that of pure polymer used in the in vivo experiment. After 7 days washout period, study agents were reshuffled between the groups so that the each group received different study agent after each wash out period.. One hour after injection, mice were placed in the corner of Open-field chamber (30 × 30 cm, Med Associates) and the locomotor activity was monitored for 15 minutes. Health condition of the mice was monitored by experienced personnel on daily basis during the whole

period of experiment. After the second treatment period animals were terminated and blood and brain were collected for adsorption and BBB penetration studies.

Determination of BT44 concentration in blood and Brain

Both blood and brain concentration of BT44 was determined 1 h after single subcutaneous injection of 50 mg/kg of nanoformulated BT44 or BT44 dissolved in PG in mice (n = 4-6 mice per group). One-hour post subcutaneous injection, mice were anaesthetized using terminal phenobarbital injection (50 mg/kg) and blood samples (0.3–0.8 ml) were collected by cardiac puncture with surgical heart exposure (open method) followed by storage in EDTA tubes (Microvette 100K3E, Sarstedt). The plasma fraction was separated by centrifugation (3000 rpm, 5 min, 4 °C), placed on dry ice followed by storage at −72°C until analysis.

For the measurement of brain concentration of BT44, mice were transcardially perfused with an ice cold normal saline and the brain tissues were collected and snap frozen in the liquid nitrogen. The concentration of BT44 in both the plasma and brain was measured by UPLC coupled with time-of-flight mass spectrometry. The measurements were conducted by Pharmidex Pharmaceutical Services Ltd (UK, https://www.pharmidex.com/)

Statistical analysis

The statistical analysis was done using Student's t-test or one-way ANOVA with a Dunnett's or Tukey HSD *post hoc* tests in GraphPad Prism 8 (GraphPad Software Inc., USA). The differences with P values below 0.5 were considered statistically significant.

Results and discussions

Polymer synthesis and characterization

POx based ABA triblock copolymers have shown great potential to deal with difficult to solubilize drugs [36, 39]. In the majority of cases, the hydrophilic block A is pMeOx while hydrophobic block B can be from a series of linear [69, 70], branched (aliphatic POx with varying side chain lengths; C4-C9) [53, 64] or aromatic ring side chains [44, 63]. For POx based amphiphiles, it has been established repeatedly, that a that a minimal contrast in hydrophilic/lipophilic domains is beneficial [64], for high

drug loading [43, 44, 59, 62, 63, 71]. Amongst many POx based triblock copolymers [53], the most commonly explored amphiphile is A-pBuOx-A [44, 45, 50] allowing, *inter alia*, ultra-high drug loading for paclitaxel (PTX) (≈ 50 wt.%).

Taking this into account, we selected three POx based copolymers (including the thoroughly investigated pBuOx based amphiphile) [35, 42, 44, 45, 59] comprising a moderately hydrophobic block B i.e. poly(2-*n*-propyl-2-oxazoline) (pPrOx), pBuOx and poly(2-*n*-pentyl-2-oxazoline) (pPentOx) (Figure 1a) and a hydrophilic pMeOx, as block A. The solubilizing capacity of the triblock copolymers for BT44 (Figure 1b) was tested by using the thin-film hydration method (Figure 1c). All polymer amphiphiles in this study were synthesized by living cationic ring opening polymerization (LCROP) as previously described [62].

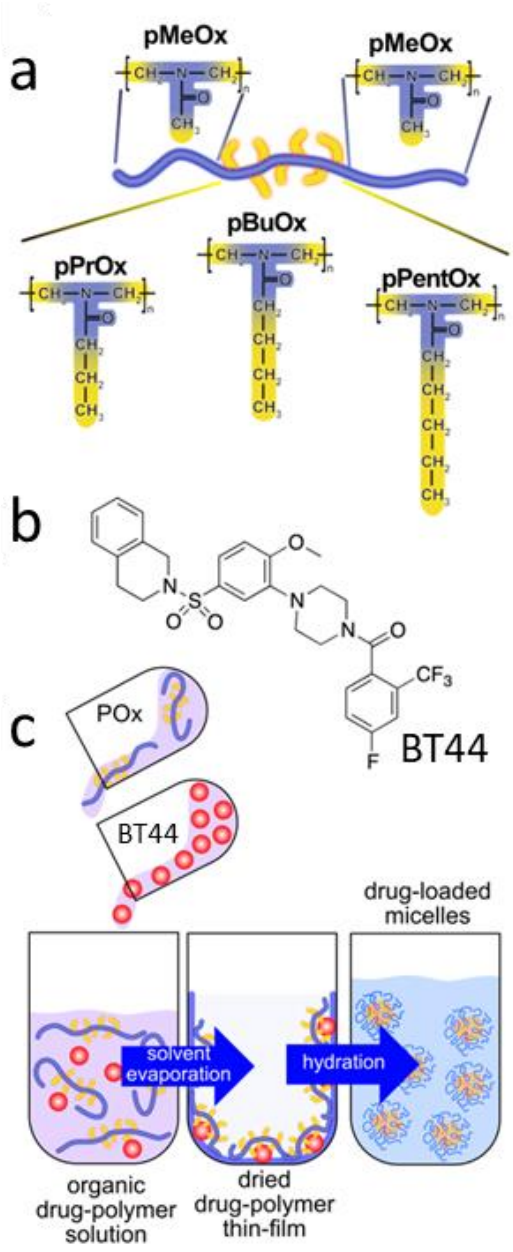

Figure 1: a) Schematic representation of the triblock copolymers used in this study. b) Chemical structure of the BT44. c) Schematic illustration of the thin-film hydration method used for the formulation development.

As all the triblock copolymers are comprised of pMeOx as A, they are represented according to the hydrophobic block i.e. A-pPrOx-A, A-pBuOx-A and A-pPentOx-A. The targeted block length for each block in the triblock copolymer is A_{35}-B_{20}-A_{35}. The former two polymers were previously investigated for drug formulation [53, 62, 69] while the A-pPentOx-A triblock copolymer was specifically synthesized for this contribution. Initially, we synthesized PentOx monomer followed by characterization with ^{1}H-NMR spectroscopy (SI; synthesis 1). All the signals were unambiguously

assigned. The signals of two methylene groups (signal 1 and 2) originating from 2-oxazoline (at 4.2 and 3.8 ppm) confirmed the successful ring formation (Figure 2a). After purification by distillation, the PentOx monomer was polymerized with MeOx (A) to obtain the desired A-pPentOx-A (supporting information: synthesis 2). The polymerization was terminated with aqueous sodium hydroxide solution. Previously, we had observed relatively little effect of the polymer termini in POx/POzi based A-B-A triblock copolymers, but this should be assessed on a case-by-case basis [69, 72]. The resulting A-pPentOx-A triblock copolymer was characterized by ^{1}H-NMR, GPC, DSC and TGA. The ^{1}H-NMR showed good synthetic control and agreement to the targeted length for individual block (Figure 2b). During synthesis, after full monomer consumption for individual block, small volume of the reaction mixture was collected and analysed by GPC. With the polymerization of each individual block, a distinct shift to higher molar mass was clearly observed and the elugrams for the intermediates and final polymer appeared essentially monomodal with reasonably low dispersity (Đ < 1.20) (Figure 2c). For the synthesis and characterization of A-pPrOx-A and A-pBuOx-A triblock copolymers, the reader is referred to previous reports [53, 62]. To understand the thermal characteristics of the novel polymer, differential scanning calorimetry (DSC) measurements were performed. Corroborating results from previously reported POx based triblock copolymers [53], all the three polymer amphiphiles exhibited a single glass transition (T_g) suggesting an amorphous sample and absence of (micro)phase separation in solid. As expected, a slight decrease in T_g was observed with the increasing side chain length in hydrophobic block i.e. 65, 63 and 58°C for A-pPrOx-A, A-pBuOx-A and A-pPentOx-A, respectively (Figure 2d and Figure S1). The thermogravimetric analysis revealed that the A-pPentOx-A remained stable and onset of the first major loss was observed at approximately 330°C (Figure 2e). Such high thermal stability could be very beneficial for melt processing, e.g. preparation of hot melt extrudates of A-pPentOx-A and drugs of interest.

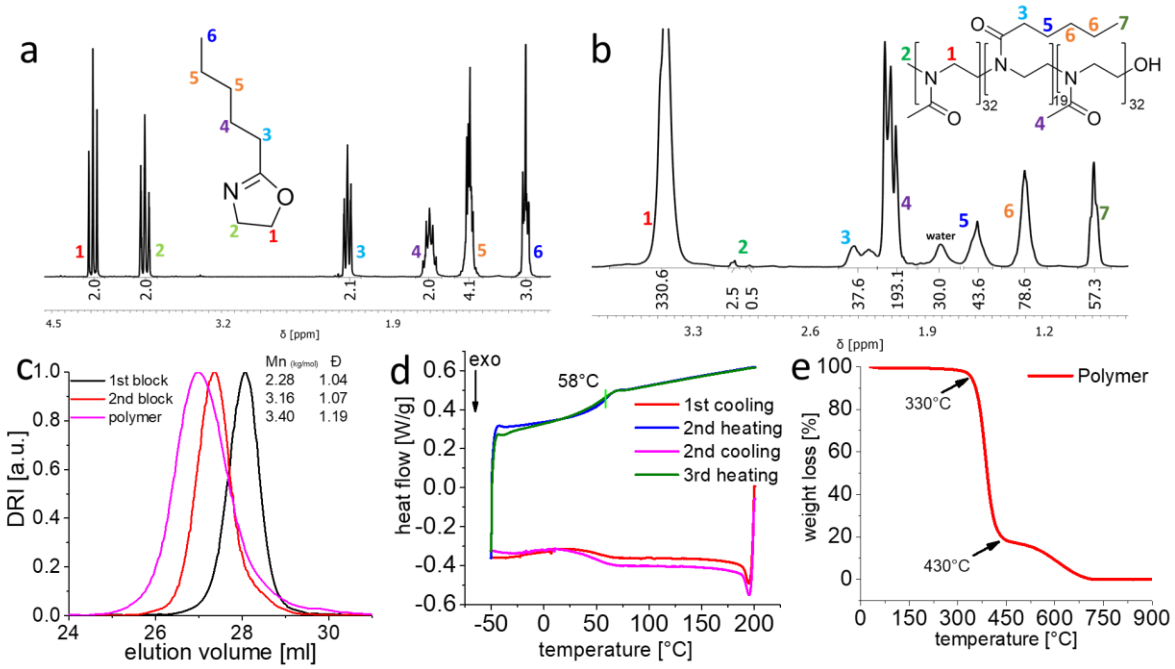

Figure 2: ^{1}H-NMR spectra ($CDCl_3$; 300 MHz; 298 K) and chemical structure of a) 2-*n*-pentyl-2-oxazoline monomer and b) pMeOx-b-pPentOx-b-pMeOx triblock copolymer with signal assignment of all major peaks. c) GPC elugrams (solvent; HFIP, system calibrated with PEG standards) after each polymerized block and purified A-pPentOx-A polymer. d) DSC thermogram of plain A-pPentOx-A triblock with heat flow occurring during the various heating and cooling cycle (10 K/min), green vertical line indicates the glass transition point at 58°C. e) Weight loss occurring during thermogravimetric analysis of A-pPentOx-A. Samples were heated from 30 to 900°C at the heating rate of 10 K/min.

Solubility parameters

The physicochemical compatibility between drug and polymer plays obviously a pivotal role in the characteristics of the formulation. The chemical structure of the drug and the polymer (backbone or side-chain) can significantly impact the drug loading and stability of the formulation [62]. Despite some attempts to "predict" drug loading [48, 53, 73], drug formulations are mostly still developed by trial and error. Considering the magnitude of the problems of hydrophobic drugs in pharmaceutical technology, finding of a universal carrier/solubilizer seems impossible [73]. There are a variety of techniques to estimate or assess the polymer-drug compatibilities [65, 74-77] in time and cost-effective manner. Here, we estimated the compatibility between BT44 and the hydrophobic block in the ABA triblock copolymers theoretically by calculating Hansen solubility parameters (HSPs) [73, 78, 79]. The HSPs values (i.e. dispersion (δ_d), polar (δ_p) and hydrogen bonding (δ_h) forces) were calculated

using the group contribution method and the molar volume was calculated by Fedor's method (Figure 3a and Table S1) [66]. Based on the principle of "like dissolves like" the distance between two materials in the 3 dimensional (3D) space can give an estimate of compatibility between two substances therefore the obtained HSPs values are depicted in 3D space (Figure 3b). Based on δ_d, δ_p, δ_h, δ_{total} values, the Flory-Huggin's interaction parameters (χ_{dp}) can be calculated, which is another measure of compatibility between polymer and drug wherein a lower value of χ_{dp} (ideally = 0) suggests a better polymer-drug compatibility. Based on the calculated χ_{dp}, BT44 compatibility with the three different hydrophobic blocks should be in the following order i.e. pPrOx > pBuOx > pPentOx indicating an inverse relationship of side chain length and polymer-drug compatibility. Specifically, pPrOx is suggested to be highly compatible (χ_{dp} ≈ 0.002) and therefore could be assumed to be the best solubilizer for BT44, while pBuOx and pPentOx gave χ_{dp} values of 0.66 and 1.50, respectively, indicative of lower compatibility. The χ_{dp} value for highly hydrophilic pMeOx was ≈ 4.26 indicating that plain pMeOx homopolymer is thermodynamically a poor solubilizer for BT44. However, this theoretical prediction represents an oversimplification of the system and the experimental solubilization of BT44 using these three amphiphiles for BT44 must be tested.

a

Solubility Parameters

polymer/drug	[a]δD	[a]δP	[a]δH	[b]δT	[c]molar volume cm³/mol	[d]Flory Huggins parameter
pPrOx	20.1	12.3	8.8	25.1	90.2	0.002
pBuOx	19.6	10.4	8.1	23.6	106.3	0.66
pPentOx	19.2	9.1	7.6	22.5	122.4	1.50
pMeOx	21.9	19.1	11.0	31.1	58.0	4.26
BT44	23.1	7.7	8.4	27.3	367.1	-

[a]Calculated by Hoftyzer and Van Krevelen's method, equation no. 4, 5 & 6, [b]calculated by equation no. 2 & 3, [c]calculated by Fedor's method, [d]calculated by equation no.1.

b

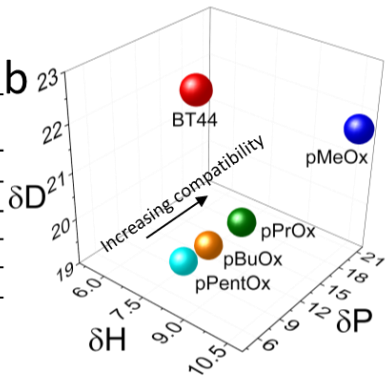

Figure 3: a) Hansen solubility parameters, molar volume and Flory Huggins parameters of BT44 and various blocks of the ABA triblock copolymers. b) Distribution of solubility parameters for BT44 and various blocks of ABA triblock copolymer in three dimensional Hansen space.

Formulation development

Previously, we had observed that a minor change such as shifting of one methylene unit from the side chain to the polymer back-bone (with in hydrophobic block) has significant impact on the loading capacity for hydrophobic drugs indicative of strong polymer/drug specificities [62]. While in the present contribution the hydrophobic blocks with the increasing side chain length i.e. C3, C4 and C5 were selected and compared for drug loading capacities.

Accordingly, the solubilisation of BT44 was tested with the three triblock copolymers with minimal to moderate amphiphilic contrast (difference of hydrophobicity in hydrophilic and hydrophobic block of the triblock copolymer). Briefly, the polymer and BT44 ethanolic solutions were mixed in desired ratios (in all cases, the polymer concentration was kept constant at 10 g/L, while BT44 concentration was increased from 2 to 10 g/L, unless otherwise stated) followed by ethanol removal and subsequent hydration of resultant thin-film by deionized (DI) water. The (dissolved) BT44 in the micellar formulation was quantified by HPLC (Figure S2), after removal of (if any) non-solubilized drug by centrifugation.

Instead of A-pPrOx-A as predicted by solubility parameters or A-pBuOx-A, proven to be the best solubilizer for many drugs [35, 45, 50, 59], unexpectedly, A-pPentOx-A gave the highest LC for BT44 (LC ≈ 47 wt.%). Increasing the BT44 feed from 2 to 10 g/L, raised the LC from 14 to 47 wt.% (1.7 to 9.0 g/L) (Figure 4a, blue bars). At the highest LC of 47 wt.%, BT44 formulation appeared as clear solution with low viscosity (Figure S3a). The LE at all the tested ratios of BT44 ranged between 80 to 90 % (Figure 4a, blue squares). For *in vitro* biological activity (or cytotoxicity) studies relatively low drug concentrations are required (typically nano- to micromolar range) but when it comes to *in vivo* studies, typically a high dose is required due to the incomplete absorption and (often) large volume of distribution (e.g. volume of distribution of BT44 is equal to 4.6 L/kg). In addition, ultra-high drug loaded formulations are favorable, particularly for injectable administration, because of limitation of injectable volume, in particular in mouse models. Previously, Lübtow et al. observed that increasing the polymer feed from 10 to 50 g/L aided to increase the aqueous solubility of curcumin (CUR) from 11 to 55 g/L, respectively [43]. Following this, an additional formulation with higher A-pPentOx-

A/BT44 feed i.e. 100/20 g/L was also prepared. This formulation provided us BT44 aqueous solubility of around 19.3 g/L. However, because of the high polymer feed, the resulting LC was only 16 wt.%, albeit with a high LE of 96% (Figure 4b).

In the case of A-pBuOx-A triblock (at 10 g/L polymer feed) the highest achieved LC was 19 wt.% (≈ 2.4 g/L at 10/8 g/L feed) (Figure 4a, red bars). Increasing the BT44 feed did not significantly improve the LC i.e. lying in the range of 4 to 19 wt.% at all the tested ratios. In contrast, LE kept on decreasing with the increasing BT44 feed i.e. 35 to 15 % (Figure 4a, red squares). The A-pPrOx-A triblock appeared to be a poor solubilizer for BT44 (LC ≈ 0.5 wt.%), at all the tested ratios (Figure 4a, black bars), the flakes of undissolved A-pPrOx-A/BT44 films were clearly visible with the naked eye (Figure S3b) during formulation experiments. In summary, formulation results showed a clear decrease in LC in order of A-pPentOx-A > A-pBuOx-A > A-pPrOx-A with loading capacities of 47wt.%, 19wt.%, 0.5wt.%, respectively (Figure 4a).

Comparing the experimental formulation results (i.e. LC for A-pPentOx-A > A-pBuOx-A > A-pPrOx) with the theoretical polymer-drug compatibility results (i.e. pPrOx > pBuOx > pPentOx) obtained by solubility parameters, it is clear that the HSPs gave completely opposite and unsatisfactory results. It is obvious that HSPs is unsuitable tool for compatibility prediction in the present systems. The predictive power of solubility parameters (δ_d, δ_p, δ_h, and δ_{total}) is based on relatively straight forward mathematical calculations [66, 78], limiting the precise prediction of the overall polarity and hydrogen-bonding ability of molecules. In addition, the interplay between hydrophilic/lipophilic domains and cargo in a solution is much more complex which can lead to differing deviations from predicted interactions [24-27, 80] in turn compromising the predictive power of solubility parameters [53]. We are aware that in the past several authors have claimed that HSPs are well suited for the prediction of polymer-drug compatibilities [73, 81], including in POx-based block copoylmers [82], but our results presented here and before [44, 53] clearly show that one has to be very careful not to overgeneralize.

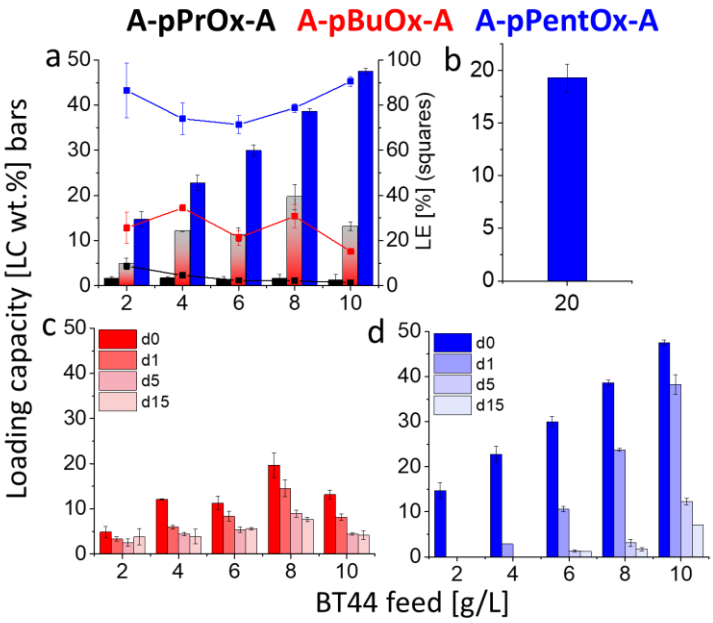

Figure 4: Maximum loading capacity (LC, bars) and loading efficiency (LE, squares) obtained with a) A-pPrOx-A (black), A-pBuOx-A (red) and A-pPentOx-A (blue) at constant polymer feed of 10 g/L, with increasing BT44 feed from 2 to 10 g/L and b) with A-pPentOx-A/BT44 feed of 100/20 g/L. Stability study of the c) A-pBuOx-A and d) A-pPentOx-A based BT44 formulation stored at ambient conditions (day 0 to 15) with constant polymer feed of 10 g/L. Data is given as means ± SD (n=3).

Stability studies

For pharmaceutical development and commercialization, the stability of the formulation is one of the basic requirements. To investigate the shelf life of BT44 formulations, the freshly prepared formulations were stored at room temperature with the initial precipitate and samples were collected at day 0, 1, 5 and 15. Previously we had observed that the A-pBuOx-A/PTX formulation exhibited an excellent stability for several months [42, 69] however, in few cases the formulation with similar amphiphiles were found to be less stable [48]. A-pPrOx-A/BT44 formulation was not included in this study because of the poor drug loading (LC ≈ 0.5 wt.%). Unlike stable A-pBuOx-A/PTX formulation, BT44 formulation with A-pBuOx-A was found to be less stable and in the course of time a gradual decrease in LC was observed in all the tested ratios e.g. the highest LC obtained with A-pBuOx-A/BT44 feed of 10/8 g/L decreased from 19 (at day 0) to 7 wt.% (at day 15) (Figure 4c, red bars).

Interestingly, in the case of A-pPentOx-A, a direct relationship between LC and formulation stability was observed i.e. formulation with high LC were found to be relatively more stable (Figure 4d). The

formulations with 2 g/L BT44 feed precipitated completely within 24 h, while the formulations with 4 to 6 and 8 to 10 g/L BT44 feed precipitated completely by day 5 and 15, respectively. The present findings are opposite to our previous results, where mitotane (MT) based formulation with A-pBuOx-A polymer (for adrenocortical carcinoma) was found to be more stable at lower MT feed (2 and 4 g/L). However, at a certain threshold MT feed (≥ 6 g/L), a rapid crystallization of MT was observed corroborated by clear melting peak in DSC thermogram of the precipitate [44]. To investigate the reasons for A-pPentOx-A/BT44 formulation instability i.e. whether BT44 crystallizes or the formulation is colloidally unstable, the formulations were further characterized by various techniques.

Physico-chemical characterization of formulation

As previously explained, the interactions between drugs and the hydrophilic corona of polymers micelles are becoming more evident, which can either lead to high drug loading [27, 80] or colloidal instability of the formulations [64], but also affect endocytosis [83-85]. The limited colloidal stability is evidenced by the fact that the resultant precipitate not only contains the drug but also the otherwise highly water soluble polymer [25, 43]. To evaluate this for the present formulations, the A-pPentOx-A/BT44 (100/20 g/L) formulation was prepared. After centrifugation, the supernatant and the sediment were separately collected and lyophilized. For better comparison, the ^{1}H-NMR spectra of the pristine BT44, plain A-pPentOx-A polymer and the (lyophilized) precipitate in chloroform-D ($CDCl_3$) as non-selective solvent (no micelles formation) were obtained (Figure S4). The ^{1}H-NMR spectra of plain polymer clearly presented all the signals suggesting that polymer existed as unimers in non-aggregated form (Figure S4 green spectra) and it was also evident that the precipitate contained not only the drug but also the hydrophilic polymer (Figure S4 red spectra), corroborating our previous findings [26, 43, 86]. However, the precipitate was significantly enriched in BT44 compared to the formulation**.**

To gain more insights into the BT44 formulations, ^{1}H-NMR experiments were further performed using deuterium oxide (D_2O) as selective solvent (micelles formation). Initially the ^{1}H-NMR spectra of all the three triblock copolymers used in this study were obtained (at concentration of 10 g/L) (Figure S5).

The A-pPrOx-A copolymer exhibited all the signals from hydrophilic as well as the more hydrophobic block (Figure S5 blue spectra, signals 1 to 6). This shows that polymer existed as unimers in D_2O because of very low amphiphilic contrast, unable to self-assemble to form micelles. This could be expected, as the pyrene assay previously also indicted no formation of micelles at 10 g/L concentration for A-pPrOx-A triblock copolymer [53]. Lübtow et al. also observed the similar behaviour for poly(2-*n*-propyl-2-oxazine) based triblock copolymer (A-pPrOzi-A) and the micellization was only induced in the presence of hydrophobic molecule i.e. CUR. Additionally, at ultra high CUR loading (LC > 50 wt.%), the signals from the more hydrophobic block were still visible, albeit with lower intensities (in D_2O), while the CUR signals were completely attenuated [43].The ^{1}H-NMR spectroscopy also revealed a similar pattern for PTX [80] and atorvastatin (ATV) [86] loaded A-pBuOx-A and A-pBuOzi-A ((poly(2-*n*-butyl-2-oxazine)) micellar formulations, respectively. However, in the absence of drug, small angle neutron scattering (SANS) revealed that the plain A-pBuOzi-A polymer existed as spherical self-assemblies without well-defined core-shell architectures. In contrast, the plain A-pBuOx-A displayed core-shell morphology [27]. The ^{1}H-NMR spectra of A-pBuOx-A [53] also exhibited all the respective signals including the hydrophobic block (Figure S5 green spectra, signals 1 to 7). Herein, the ^{1}H-NMR spectra of the plain A-pPentOx-A (Figure S6 green spectra) and the lyophilized BT44 formulations (Figure S6 red spectra) were also obtained in D_2O. In both spectra, the signals corresponding to the hydrophobic block were completely absent (Figure S5, red spectra, signals 3, 5, 6 and 7), additionally no signals from the BT44 were visible in the formulation. In contrast, Hiller et al. observed all the representative signals (^{1}H-NMR) from their diblock i.e. $pMeOx_{17}$-$pPentOx_3$ including the signals from hydrophobic pPentOx in D_2O [87]. However, in comparison to present A-pPentOx-A triblock copolymer, Hiller et al. had a very short hydrophobic block (3 repeat units) and resulting very low amphiphilic contrast. The complete disappearance of signals from hydrophobic block (in plain A-pPentOx-A triblock) indicates short transverse relaxation time (T_2) and suggests micelles with a rigid core both in the presence and absence of BT44. The direct comparison of A-pBuOx-A and A-pPentOx-A micellar formulations utilizing the analytical tools like solid state NMR [25, 80] and SANS could give

us much deeper understanding of polymer drug interactions resulting in the different micellar structure and dynamics, however such analysis is beyond the scope of current contribution. In order to investigate the reasons for the poor stability of A-pPentOx-A/BT44 formulation, DSC analysis was performed to evaluate, whether the precipitation is associated with BT44 crystallization similar to previously reported MT-formulation [44] or because of colloidal instability, agglomeration and sedimentation. Initially the DSC thermogram of the pristine BT44 was obtained to determine the melting point (Figure S7a). The sharp endothermic peak at 146°C in the first heating cycle indicated the crystalline nature of BT44 (Figure S7a black curve) while the DSC traces in the second and third heating cycle did not show any melting peaking, as BT44 remained in its amorphous form with a T_g of 75°C (Figure S7a, green vertical line). In this regard, only the first heating cycle in the DSC thermograms of pure BT44 and the resultant precipitate in formulation (i.e. A-pPentOx-A/BT44 at 10/4 g/L feed) at day 5 were compared (after lyophilization). Unlike pristine BT44, no melting peak was observed in the precipitate at day 5 confirming BT44 amorphous nature (Figure S7b red curve) corroborating our previous findings [32, 42], suggesting that the poor stability can be correlated to micellar agglomeration and sedimentation.

In the pharmaceutical product design, the formulation instability is a serious risk factor which can limit their wide spread use. Lyophilisation is generally a primary strategy to improve the shelf life of a drug product. Therefore the A-pPentOx-A/BT44 100/20 g/L formulation was prepared (Figure 4b) and lyophilized. During storage, the physico-chemical stability of the lyophilized formulation is also one of the quality attributes that should be evaluated. Such formulations have the tendency to crystalize during handling, storage or transportation. In order to investigate this, the DSC thermograms of pure polymer, pristine drug and the lyophilized formulation after 15 days of storage at room temperature were compared (Figure 5a). The absence of a melting peak (at 146°C) in the first heating cycle indicated that the BT44 remained as amorphous form in lyophilized formulation (Figure 5a blue curve) while in second and third heating cycle, unlike pristine BT44 (T_g at 75°C, Figure S7a) a single T_g was

observed at 58°C (Figure S8) which corresponds to the T_g of plain A-pPentOx-A polymer indicative of complete miscibility of the drug and polymer.

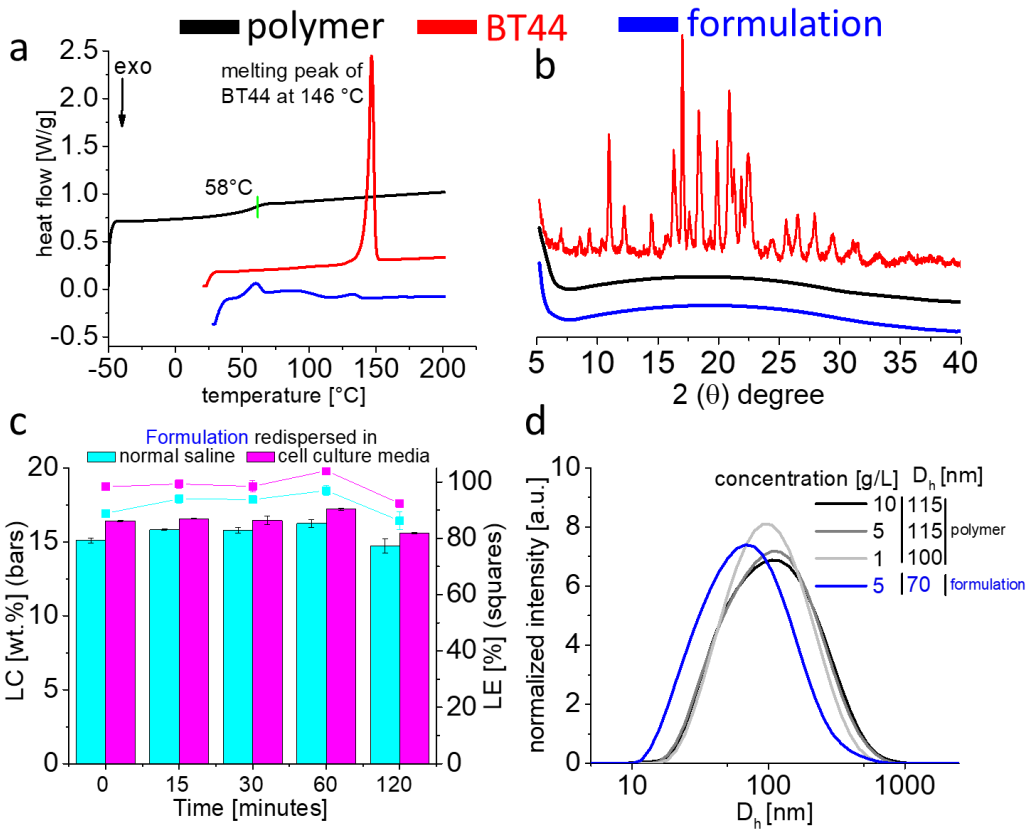

Figure 5: a) DSC thermograms (at heating rate of 10 K/min) of pristine BT44 (red, first heating cycle, sharp melting peak at 146°C), plain polymer (black, second heating cycle, T_g at 58°C) and lyophilized formulation (blue, first heating cycle, absence of melting peak for BT44), respectively after 15 days of storage at room temperature. b) Powder-XRD spectra of pristine BT44 (red), plain polymer (black) and lyophilized formulation (blue) after one month of storage at room temperature. c) Redispersion of lyophilized formulation (polymer/BT44 100/20 g/L) after 30 days of storage at room temperature in normal saline (blue) and cell culture media (magenta) for short term stability studies from time 0 to 120 minutes. Data is given as means ± SD (n=3). d) The size distribution by intensity (measured at 173° scattering vector) of plain polymer (10, 5 and 1g/L) and BT44 formulation (5 g/L) redispersed in normal saline (filtered through 0.45 µm PVDF filter).

For further analysis, the pristine BT44, plain polymer and lyophilized formulation after 30 days of storage at room temperature were analysed by powder-XRD (Figure 5b). The diffractograms of the pristine BT44 showed multiple peaks in the 2Θ range of 10 to 35° showing the crystalline nature of BT44 (Figure 5b, red curve). In contrast, the broad halos in the plain polymer and lyophilized formulation indicate their amorphous nature (Figure 5b black and blue curve, respectively). This

preliminary stability study using DSC and powder XRD analysis suggests that such formulations can be stored reasonably well, as lyophilized powder without a high risk of recrystallization. However, more detailed studies at different temperature and relative humidities will be needed to complete the picture. In addition, the analysis of traces of crystallinity via multimodal non-linear imaging would be of interest [88].

For lyophilized formulations, the complete redispersion or aqueous reconstitution is also a very important step for parenteral administration. In addition, the evaluation of short-term stability of the redispersed formulation is relevant in practical settings. The final redispersed formulation should remain stable for some time to conveniently allow for parenteral administration (injection or infusion), potentially to different patients over some limited time. Previously, lyophilized POx based PTX, CUR, ATV and MT formulations (without any additional cryo-/lyoprotectants) displayed excellent redispersibility before use [43, 44, 86]. In this regard, A-pPentOx-A/BT44 100/20 g/L lyophilized formulations (after storage at room temperature for 30 days) were redispersed in normal saline and cell culture media (without serum) and quantified at time 0, 15, 30, 60 and 120 minutes by HPLC to determine the short-term storage. Upon redispersion (at t = 0 min) with normal saline, initially a negligible decrease in LC (i.e. 16 to 15 wt.%) was observed while with cell culture media, 100 % redispersibility was noticed (LC ≈ 16 wt.%). In the time course of 120 minutes, the LC of normal saline and cell culture media based formulations decreased slightly to 14 and 15 wt.%, respectively, and accordingly, a minor precipitation was noted. From the redispersion results, it can be concluded that A-pPentOx-A/BT44 formulations can be stored as lyophilized powder but needs to be used timely after redispersion.

To estimate the size of assemblies, redispersed formulations (in normal saline) were characterized by dynamic light scattering (at 173°) at room temperature. Initially, the self-assemblies of plain A-pPentOx-A polymer at different concentrations (10, 5 and 1 g/L) were measured and the size (hydrodynamic diameter, D_h) fell in the range of 100-115 nm. However, upon incorporation of BT44 (5 g/L), the D_h decreased to approximately 70 nm indicative of BT44 induced reorganization and

compaction of the self-assemblies. However, it should be clear that the size of these self-assemblies are beyond the size to be expected for simple, spherical polymer micelles, as the theoretical extended chain length of the polymers is well below 40 nm.

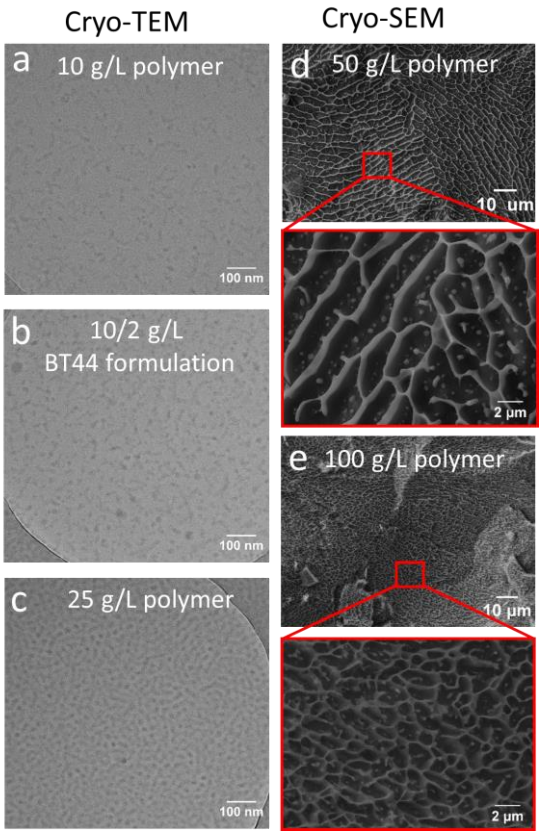

Figure 6: The cryo-transmission electron microscopy analysis (cryo-TEM) of a) 10 g/L plain A-pPentOx-A polymer, b) 10/2 g/L A-pPentOx-A/BT44 formulation, c) 25 g/L plain A-pPentOx-A polymer. The cryo-scanning electron microscopy (cryo-SEM) analysis of d) 50 and e) 100 g/L plain A-pPentOx-A polymer (acceleration voltage ETH: 8kV).

To gain more insights into the size and morphology of the assemblies, initially, we visualized the plain polymer solutions (at concentration of 10 and 25 g/L) and polymer/BT44 (10/2 g/L) formulation by cryo-TEM. The results revealed the presence of some short worm-like assemblies (Figure 6a). This can explain the higher D_h observed by DLS i.e. 100-115 nm (at 10 g/L plain polymer solution). No notable differences were observed in morphology, when plain polymer was compared to the BT44 formulation (at polymer/BT44 10/2 g/L) (Figure 6b). When the polymer concentration increased from 10 to 25 g/L, the overall population of the worms also increased and the whole grid seemed to be saturated with these assemblies (Figure 6c). The alignment, range of intermediate structures and further branching

between the worms is indicative of a dense network formation. Generally, the transition to higher-order assemblies can be correlated to increase in viscosity. In this regard, by cryo-TEM, Hahn et al. observed the morphological transition from spherical micelles to worm like network causing the macroscopic gelation for poly(2-phenyl-2-oxazine) based A-B-A (A-pPheOzi$_{15}$-A) triblock copolymer (at 200 g/L concentration) [89]. However, similar polymer with a shorter hydrophobic block (A-pPheOzi$_5$-A), which remain liquid, also exhibited lamellae like structures in cryo-SEM analysis at higher concentrations. Here, both the A-pPentOx-A/BT44 formulation and the plain polymer solution, appeared as free flowing liquid at all the tested concentrations. To obtain further insights into the morphology of A-pPentOx-A plain polymer solutions at 50 and 100 g/L, the visualization was performed by cryo-SEM. Similar to the case of A-pPheOzi$_5$-A, the 50 g/L A-pPentOx-A polymer solution also exhibited lamellae like structures (Figure 6d) which were further condensed by increasing the polymer concentration to 100 g/L (Figure 6e). This further condensation lead to structural transition to honeycomb like structure. To the best of our knowledge this is the first study presenting the worm like morphological details of any pPentOx based triblock copolymer and its drug formulation. However, previously the worm like structures have been reported for A-pPrOzi-A/CUR [43] and A-pBuOx-A/cisplatin/etoposide formulations [59] while in the presence of PTX, A-pBuOx-A exhibited raspberry like micelles [31]. The plain A-pPrOzi-A existed as unimers [43] while plain A-pBuOx-A polymer solution exhibited spherical micelles along with the presence of few worm like assemblies [31]. Recently, depending upon the drug feed, Lim et al. observed the transition of freshly prepared A-pBuOx-A/Olaparib spherical micelles ($D_h \approx$ 10-30 nm) to worm like structures ($D_h \approx$ 200 nm) in the time span of 72 hours [90]. The authors further suggested that the spherical micelles can be therapeutically more efficient for systemic delivery of anticancer drugs when compared to worm like assemblies. However, this should be verified on case-by-case basis, because the nature of hydrophobic block, overall hydrophilic lipophilic balance, chemical nature of drug and the drug feed are the major driving forces for such kind of transitions, which might result in loosely or densely packed micellar architectures, resulting in rapid or slow release of drugs.

In vitro and In vivo studies

Assessment of polymer cytocompatibility by Alamar blue assay.

To be suitable for preclinical development and clinical translation the excipients used for formulation development must be nontoxic. We, therefore, evaluated cytocompatibility of the polymer in vitro using Alamar blue assay. However, the POx based amphiphiles have been repeatedly established cytocompatible several times in vitro and in vivo studies [31, 43-45]. In this regard, we have also performed the cytocompatibility studies of the A-pPentOx-A based triblock copolymer in MG87 RET cells. The cells were exposed to 1-50 g/L of polymer for 72 hours. We observed a polymer concentration dependent decrease in cell viability with respect to the vehicle (untreated) cells($p<0.0001$, ANOVA with Dunnett's posthoc) (Figure 7a). At 1 g/L, no reduction in cell viability was observed, while a minor reduction was observed at the cells treated with 10 g/L of polymer ($p=0.0001$, ANOVA with Dunnett's posthoc). In contrast, at 50 g/L of polymer, cell viability dropped well below 50 % of control ($p<0.00001$, ANOVA with Dunnett's posthoc). Previously, we have seen no considerable cytotoxicity for a variety of POx based AB and ABA triblock copolymers. However, it should be kept in mind that this is expected to depend on the cell type and these concentrations are very high, by 1-2 orders of magnitude exceeding commonly investigated once In addition, some discrepancies in the cytotoxicity assessment might be also related to the differences in experimental methods (MTT/WST vs Alamar Blue assay).

Biological activity of BT44 formulation in immortalized cells

GDNF family ligands signal through GFRα/RET complex (Airaksinen and Saarma, 2002). Previously, it has been shown that RET agonists BT13 and BT44 stimulate RET phosphorylation and RET-dependent downstream intracellular signaling (Mahato and Sidorova, 2020; Mahato et al., 2020; Renko et al., 2021; Viisanen et al., 2020). Therefore, in the present study we evaluated the ability of nanoformulated BT44 to activate RET and RET-dependent downstream signaling in MG87 RET fibroblasts transfected with GFRα1 by Western blot and using a reporter gene-based assay.

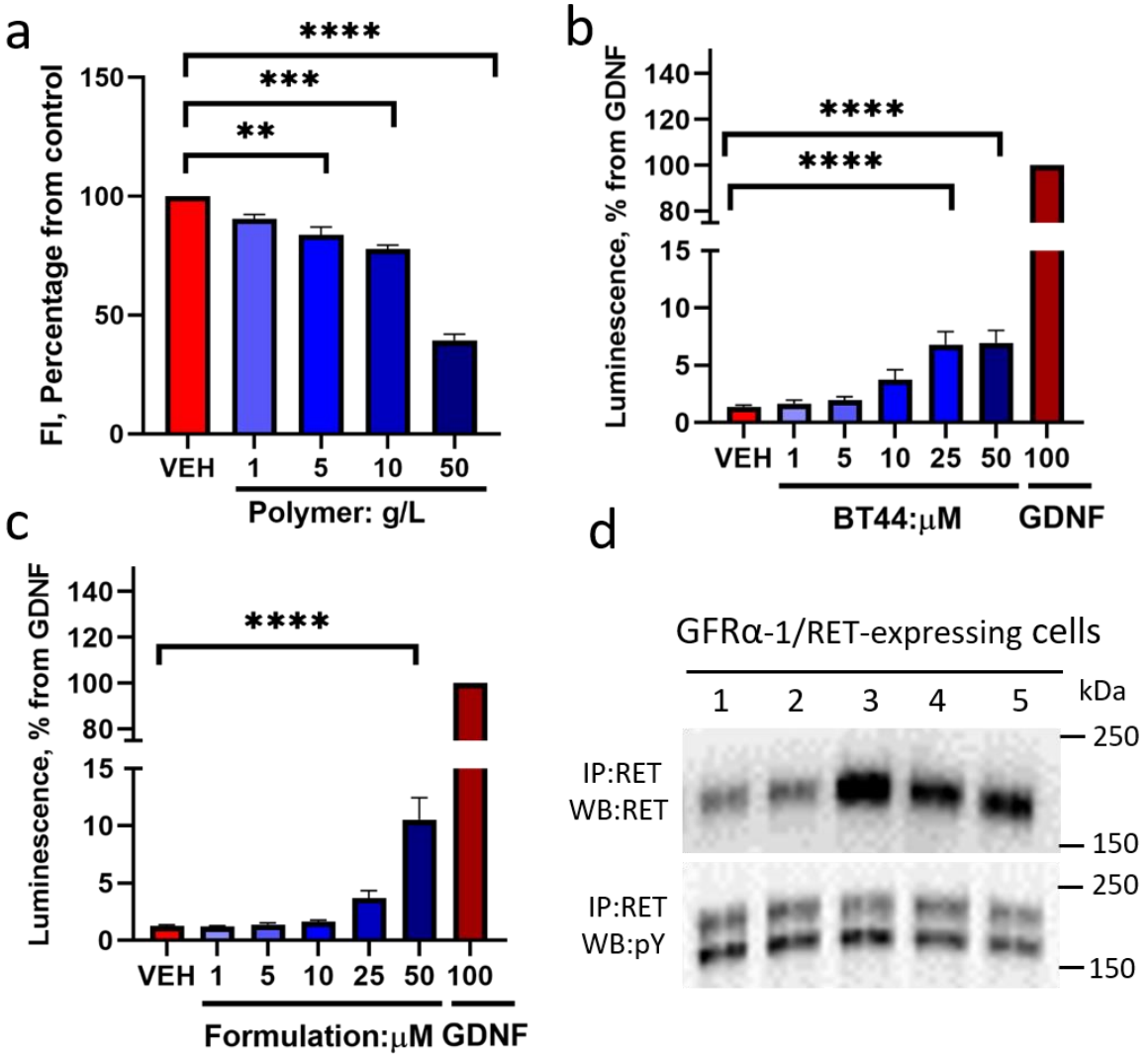

Figure 7: a) Cytotoxicity study of the plain polymer (A-pPentOx-A) at various concentrations, studied by Alamar blue assay after 72 hour of incubation with MG87 RET cells. The quantitative data are presented as mean ± SEM. (VEH; vehicle, cell culture media, FI; Fluorescence Intensity, ANOVA with Dunnett's post-hoc test compared to vehicle, n = 4; ** P < 0.01, *** p < 0.001, **** p < 0.0001). b) BT44 and c) nanoformulated BT44 (at various concentrations) induced luciferase activity in reporter gene-based assay. d) Assessment of RET phosphorylation by Western blotting in GFRα1-transfected MG87 RET cells. Lanes 1, 2, 3, 4 and 5 are VEH (1% DMSO in DMEM), plain polymer, BT44 nanoformulation, BT44 and GDNF respectively. The quantitative data are presented as mean ± SEM. Concentrations provided are in ng/ml for GDNF and µM for polymer, nanoformulation and BT44. (IP; immunoprecipitation, WB; Western blotting. **** p < 0.0001 one-way ANOVA with Dunnett's *post hoc* test, Number of experiment (n)=3–4).

The BT44 nanoformulation increased the luciferase activity at 50 µM (Figure 7c) in the reporter cell line by 8.4 fold (p<0.0001, ANOVA with Dunnett's posthoc). In line with previously published results,

non-formulated BT44 (Figure 7b) increased the luciferase activity both at 25 and 50 µM by 8.9 fold ($p<0.0001$, ANOVA with Dunnett's posthoc). GDNF was used as positive control and data was normalized to the signal elicited by GDNF. In line with reporter gene-based assay results, nanoformulated BT44 increased the level of phosphorylated RET in GFRα1 transfected MG87 RET cells compared to both vehicle and plain polymer (Figure 7d). These data indicate that POx based BT44 formulation retained the ability to activate RET.

Neuroprotective properties of BT44 formulation in dopamine neurons

Previously, it has been shown that both BT13 and BT44 promote the survival of cultured dopamine neurons and also protect these neurons from dopamine neurotoxin induced cell death (Mahato et al., 2020; Renko et al., 2021). Therefore, we also tested the ability of nanoformulated BT44 to protect dopamine neurons against N-methyl-4-phenylpyridine (MMP+) induced cell death. MMP+ is neurotoxin that inhibit the complex I of the mitochondria leading to the depletion of adenosine triphosphate (ATP) eventually cell death. At 100 nM, nanoformulatedBT44 increased the number of TH-positive neurons by 1.9 fold ($p= 0.0103$) which is comparable to the effect produced by BT44 dissolved in 1% DMSO (2.2 fold increase, $p=0.0050$) and GDNF (2.2 fold increase, $P=0.0040$) ($p= 0.0013$, ANOVA with Dunnett's post hoc test for all comparisons) (Figure 8a). Thus, the nanoformulation did not negatively affect neuroprotective properties of BT44.

Interacton of formulated BT44 with GDNF receptors

Further, we studied the binding of nanoformulated BT44 with GFRα1 and GFRα1/RET using MST and cell-based iodinated GDNF displacement assay. The binding of neurotrophic factors GDNF to GFRα1 and activation of RET receptors has been investigated in various laboratories (Jing et al., 1996; Klein et al., 1997; Treanor et al., 1996). The GDNF binds to the soluble form of GFRα1 with Kd of 630 pM as shown by surface plasmon resonance binding studies (Cik et al., 2000). Using MST assay, we observed a somewhat lower binding affinity of GDNF to GFRα1 (Kd = 260 nM, data not shown), thus validating the assay. Formulated BT44 also binds to GFRα1, although, expectedly, with much lower affinity (Kd = 3.6 ± 2.2 µM) (Figure 8b). GDNF is a rather big protein molecule which forms multiple contact with

GFRα1, while compounds belonging to BT scaffold make only a few hydrogen bonds and other contacts with aminoacid residues of GFRa1 (Ivanova et al., 2018). Therefore, higher Kd of BT44 compared to that of GDNF in GFRa1 binding assay is expected. Importantly, binding of formulation to GFRα1 in the presence of RET was not observed, rather aberrant MST traces were seen due to protein aggregation. Here we speculate that aggregates observed in this assay might be due to the complex formation between GFRα1, the nanoformulation and RET. Further studies are needed to verify this hypothesis.

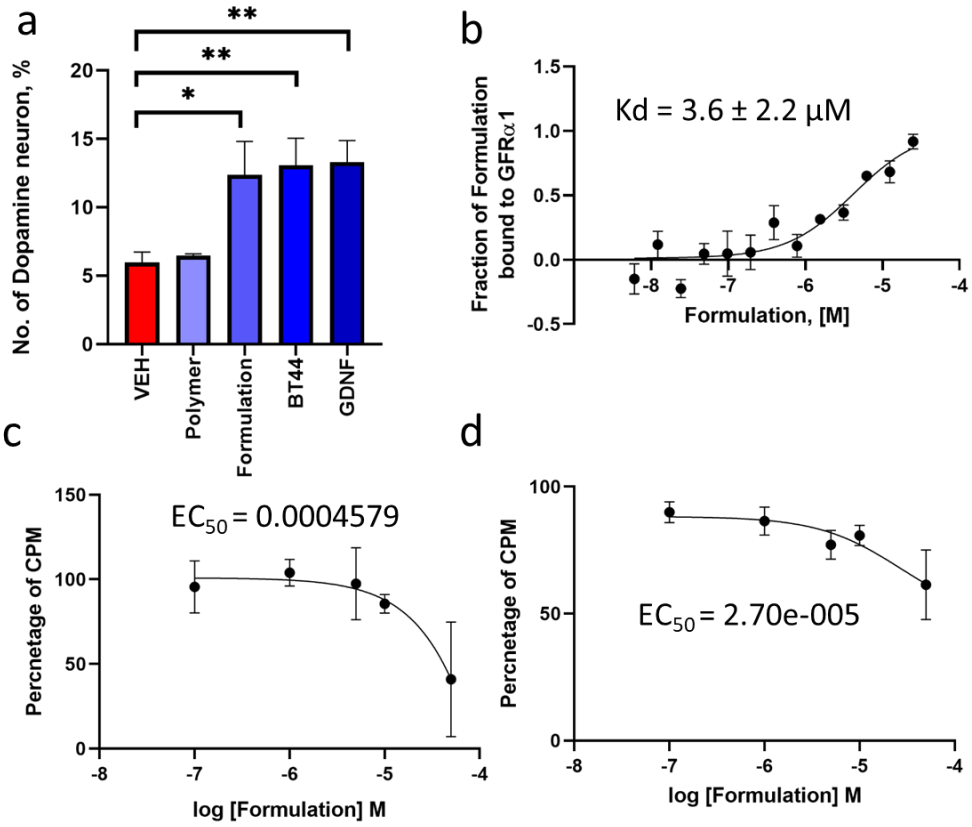

Figure 8: a) The BT44 nanoformulation protected cultured dopamine neurons from MMP+ neurotoxin induced cell death. The number of TH-positive cells in the wild-type midbrain cultures exposed with MPP+, vehicle, plain polymer, nanoformulated BT44, BT44 or GDNF, respectively, on 6th day in vitro normalized to the total number of cells in the culture and presented as percentage of vehicle (1% DMSO in DMEM F12 media)-treated samples, average from 4 independent experiments. The concentration of BT44, plain polymer and nanoformulation is given in nM, concentration of GDNF used as a positive control is provided in ng/ml. The quantitative data are presented as mean ± SEM (VEH; Vehicle, 1% DMSO in DMEM F12 media. * $p < 0.05$, ** $p < 0.01$, one-way ANOVA with Dunnett's *posthoc* test). b) The binding of nanoformulated BT44 (0–10 µM) to GFRα1 (20 nM) monitored by MST. c,d) Displacement of 50 pM ^{125}I-GDNF from GFR α1 (c) GFR α1/RET complex (d) by

nanoformulated BT44. Each data points represents mean ± SEM of 2-4 independent repeats. The binding isotherms were fitted using nonlinear regression.

We also performed competition-binding studies with formulated BT44 in cells expressing GFRα1 or GFRα1/RET. In this assay, nanoformulated BT44 displaced radiolabeled GDNF with IC_{50} value of 460×10^{-6} Min GFRα1 transfected cells (Figure 8c) and 27×10^{-6} M (Figure 8d) in GFRα1/RET transfected cells. When GFRα1 was co-expressed with RET at a DNA ratio of 1:1, the potency of the nanoformulated BT44 in ^{125}I-GDNF assay was higher compared to that observed in the cells expressing only GFRα1. A similar trend was also observed for GDNF in GFRα1-expressing cells, wherein unlabeled GDNF displaced ^{125}I-GDNF with a IC_{50} of $1.9 \pm 0.2 \times 10^{-9}$ M, while in GFRα1/RET transfected cells (1:1 DNA ratio) an IC_{50} of $10.6 \pm 2.1 \times 10^{-12}$ M for the high affinity site and $2.3 \pm 1.1 \times 10^{-9}$ M for the low affinity site (Cik et al., 2000) was found. Overall, our *in vitro* studies suggest that nanoformulated BT44 has similar effects to that of free BT44 and GDNF in several important assays n a several assays.

Evaluation of absorption, BBB penetration and acute toxicity of BT44 formulation

In our previous *in vivo* studies, we used PGas a vehicle for the BT44 administration, due to poor aqueous solubility of BT44 (Renko et al., 2021; Viisanen et al., 2020). In rats, PGdid not show any significant toxicity after both subcutaneous and intracranial administration. However, the absorption of BT44 into blood stream after subcutaneous injection of the compound dissolved in PGwas found to be rather low (Viisanen et al., 2020). After intravenous administration a portion of BT44 (approx. 18%) also penetrated through the BBB (Renko et al., 2021). Herein, we investigated whether a higher absorption and potentially even better BBB penetration can be achieved with the nanoformulated BT44 after subcutaneousadministration.

The plasma and brain concentrations of BT44 were measured one hourpost injection and found significantly higher in the case of nanoformulated BT44, compared to PGbased solution (6.6 fold, p=0.0001 and 13 fold, p=0.0094, respectively) (Figure 9a and 9b). Apparently, nanoformulated BT44 did not only increase absorption of BT44 into blood stream, but also improved BBB penetration of the compound, as the relative increase of BT44 concentration was two times higher in brain than in plasma. Very recently, Hwang et al. also observed the similar effect by using A-pBuOx-A/vismodegib

(VSM) based nanoformulation, as VSM concentration was found to be much higher in medulloblastoma and forebrain of the mice compared to the free drug. The authors hypothesized that the encapsulation of VSM in carriers reduced its interaction with plasma proteins, hence increasing the availability of free VSM leading to relatively higher transport across BBB [35]. Another possibility could be interference with drug efflux pumps which are prevalent in the BBB, and its role in restricting brain entry of multiple drugs is widely accepted [91-93]. However, further studies are needed to support or reject this hypothesis. Accordingly, higher transport across the BBB has also been described for nanoformulated domperidone, which normally does not cross the BBB [94-96]. In any case, the observed increase in BBB penetration is highly beneficial for CNS targeted drugs.

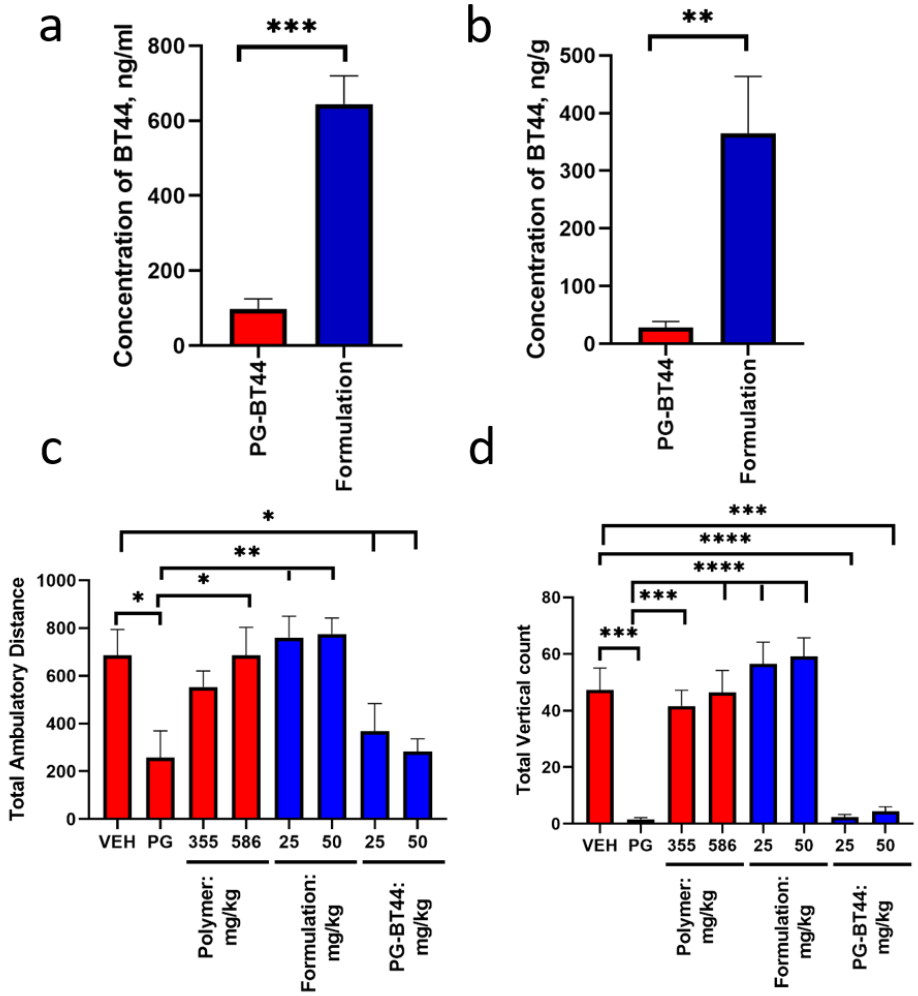

Figure 9: The plasma and brain concentrations of BT44 formulation and toxicity studies in mouse after subcutaneous administration. The plasma (a) and brain (b) concentration of BT44 after one hour PG-BT44 and formulation injection. Toxicity of formulation was monitored using behavioural parameters

such as total ambulatory distance travelled (c) and total vertical count (d) in Open Field behavioural test. Each data points represents mean ± SEM of 4-5 mice per group. * P < 0.05, ** P < 0.01, *** P < 0.001, **** P < 0.0001 one-way ANOVA with Dunnett's *posthoc* test.

Finally, we evaluated also the toxicity of nanoformulated BT44 in mice. In this regard, the locomotor and exploratory activity were assessed by the Open Field behavioral test. Additionally, the general conditions of the animals were visually monitored . To our surprise, and in contrast to experimental observations in rats, in mice the vehicle PG negatively impacted the behavior of experimental animals. Statistically significant differences were observed in motor function (both total ambulatory distance travelled and total vertical counts) between the treatment groups (p= <0.0001, one-way ANOVA) one hour post-administration of tested substances. Total ambulatory distance travelled by mice treated with PG (p= 0.0393) alone and PG-BT44 both at 25 (p= 0.0422) and 50 mg/kg (p= 0.0381) was significantly reduced compared to this characteristic for mice treated with saline (Figure 9c). Further, vertical counts were also affected by PG alone (p=0.0001) or in combination with 25 mg/kg (p<0.0001) or 50 mg/kg (p=0.0001) of BT44 (Figure 9d). The reduction in motor activity was also visually very clear in home cages. Mice receiving PG (either alone or in combination with BT44) remained immobile and practically non-reactive to handling. The effect was temporary and within a few hours pos injection (2-6 hours) the mobility of animals gradually restored. All animals that remained immobile during ≥ 2h received intraperitoneal injection of 1 ml of saline to prevent dehydration. All animals were visually normal at 24 h post treatment. Notably, the no-observed-effect level (NOEL) and maximum tolerated dose (MTD) for PG in mice when injected intraveneously are 1.036 g/kg and 1.554 g/kg respectively (Thackaberry et al., 2014). Toxicity manifestations such as hind limb ataxia, hind limb muscle contraction and hemolysis, was observed when the dose of PG exceeded MTD (Thackaberry et al., 2014). According to the information from PubChem database, lethal dose 50 (LD_{50}) of PG in mice after subcutaneous injection was equal to 17,4 g/kg, in rats – 28,8 g/kg. In the current study the dose of PG injected subcutaneously constituted 10.3 g/kg. This is below LD_{50}, but seems to be sufficient to produce some adverse effects in mice, but according to our previous studies not rats. Thus, there are

interspecies differences in sensitivity to PG, which is in line with published data (PubChem). Noteworthy, there are several reports indicating PG toxicity in humans [97, 98].

In comparison, the nanoformulated BT44 (25 and 50 mg/kg) and plain polymer (at corresponding doses of 355 and 586 mg/kg) produced no significant changes in evaluated behavioral parameters (total ambulatory distance and vertical counts) after subcutaneous injection (Figure 11 C and D). Animals receiving plain polymer or BT44 formulation also freely moved in home cages and were responsive to investigator's manipulations. These data suggest that the plain polymer excipient and nanoformulated BT44 is safe *in vivo* and could be used for future preclinical development.

Conclusion:

Herein, we present the first micellar nanoformulation of BT44 with an ultra-high drug loading. The extent and pattern of compatibility between polymer and drug when considering Hansen solubility parameters between BT44 and three amphiphiles were not in accordance with the formulation results. As has described before for other drugs, Hansen solubility parameters are not the right choice for estimating compatibility in POx based system, especially considering the fact that depending upon nature and overall load of guest molecule, the hydrophilic pMeOx may play an important role in solubility as well as stability of the system [25, 27, 80]. The POx based triblock copolymer i.e. A-pPentOx-A gave ultra-high drug loading of around 47 wt.%. The developed formulations underwent detailed physicochemical characterization. The formulation can be stored as lyophilized powder ready for redispersion. Formulated BT44 bind to its cellular receptor, retained its biological activity in immortalized cells and its neuroprotective properties in dopamine neurons. Furthermore, the absorption of formulated BT44 into the blood stream and its blood-brain barrier penetration properties were significantly improved compared to conventional preparation of the compound in PG. We did not observe acute toxicity of either a polymer or BT44 in mice.

Similar to previously reported POx based triblock copolymers formulations [35, 45, 58, 59], we anticipate that A-pPentOx-A/BT44 will allow the parenteral administration and help to alleviate the

use of toxic excipients not only at its preclinical development phase but also potentially for future clinical use.

Associated Content:

Corresponding authors:

E.mail: malik.haider@uni-wuerzburg.de

ORCID: Malik Salman Haider: 0000-0003-4248-8828

E-mail: yulia.sidorova@helsinki.fi

ORCID: Yulia Sidorova: 0000-0001-8230-0530

Notes: R.L. is listed as co-inventor on a patent pertinent to some materials in the present work and is co-founder of DelAqua Pharmaceutical Inc. intending commercial development of poly(2-oxazoline)s based drug delivery system. YS is a minor shareholder of GeneCode Ltd, a company holding patent for BT compounds.

Acknowledgement

Malik Salman Haider is grateful to higher education commission of Pakistan and German academic exchange services (HEC-DAAD Pakistan) for the award of PhD scholarship. We also thank Jan Weichhold for providing technical support during XRD measurements. We are grateful to Paula Collin for her excellent technical assistance with cell-based assays and to Pharmidex Pharmaceutical services Ltd (UK) for measuring of plasma and brain concentration of BT44. We further thank NMR core facility supported by University of Helsinki, Biocenter Finland and Helsinki Institute of Life Science (HiLIFE) for verification of the structure of BT44.

References

1. Ali, S. and K. Kolter, *Challenges and opportunities in oral formulation development.* American Pharmacuetical Review, 2012. **15**(7): p. 1.
2. Williams, H.D., et al., *Strategies to address low drug solubility in discovery and development.* Pharmacological Reviews, 2013. **65**(1): p. 315-499.

3. Durães, F., M. Pinto, and E. Sousa, *Old drugs as new treatments for neurodegenerative diseases.* Pharmaceuticals, 2018. **11**(2): p. 44.
4. Enciu, A.M., et al., *Neuroregeneration in neurodegenerative disorders.* BMC neurology, 2011. **11**(1): p. 1-7.
5. Bondarenko, O. and M. Saarma, *Neurotrophic Factors in Parkinson's Disease: Clinical Trials, Open Challenges and Nanoparticle-Mediated Delivery to the Brain.* Frontiers in Cellular Neuroscience, 2021. **15**.
6. Mahato, A.K. and Y.A. Sidorova, *RET Receptor Tyrosine Kinase: Role in Neurodegeneration, Obesity, and Cancer.* International Journal of Molecular Sciences, 2020. **21**(19): p. 7108.
7. Mahato, A.K., et al., *Glial cell line–derived neurotrophic factor receptor rearranged during transfection agonist supports dopamine neurons in vitro and enhances dopamine release in vivo.* Movement Disorders, 2020. **35**(2): p. 245-255.
8. Sidorova, Y.A., et al., *A novel small molecule GDNF receptor RET agonist, BT13, promotes neurite growth from sensory neurons in vitro and attenuates experimental neuropathy in the rat.* Frontiers in pharmacology, 2017. **8**: p. 365.
9. Viisanen, H., et al., *Novel RET agonist for the treatment of experimental neuropathies.* Molecular pain, 2020. **16**: p. 1-19.
10. Renko, J.-M., et al., *Neuroprotective Potential of a Small Molecule RET Agonist in Cultured Dopamine Neurons and Hemiparkinsonian Rats.* Journal of Parkinson's Disease, 2021(Preprint): p. 1-24.
11. Bahr, M.N., et al., *Rapid screening approaches for solubility enhancement, precipitation inhibition and dissociation of a cocrystal drug substance using high throughput experimentation.* Journal of Drug Delivery Science and Technology, 2021. **61**: p. 102196.
12. Fernandes, G.J., et al., *A review on solubility enhancement of carvedilol—a BCS class II drug.* Journal of Pharmaceutical Innovation, 2018. **13**(3): p. 197-212.
13. Singh, D., N. Bedi, and A.K. Tiwary, *Enhancing solubility of poorly aqueous soluble drugs: Critical appraisal of techniques.* Journal of Pharmaceutical Investigation, 2018. **48**(5): p. 509-526.
14. Kumar, S., et al., *Nanotechnology as emerging tool for enhancing solubility of poorly water-soluble drugs.* Bionanoscience, 2012. **2**(4): p. 227-250.
15. Chi Lip Kwok, P. and H.-K. Chan, *Nanotechnology versus other techniques in improving drug dissolution.* Current pharmaceutical design, 2014. **20**(3): p. 474-482.
16. Shetab Boushehri, M.A., D. Dietrich, and A. Lamprecht, *Nanotechnology as a Platform for the Development of Injectable Parenteral Formulations: A Comprehensive Review of the Know-Hows and State of the Art.* Pharmaceutics, 2020. **12**(6): p. 510.
17. Saka, R. and N. Chella, *Nanotechnology for delivery of natural therapeutic substances: a review.* Environmental Chemistry Letters, 2021. **19**: p. 1097–1106.
18. Cabral, H., et al., *Block copolymer micelles in nanomedicine applications.* Chemical Reviews, 2018. **118**(14): p. 6844-6892.
19. Ghosh, B. and S. Biswas, *Polymeric micelles in cancer therapy: State of the art.* Journal of Controlled Release, 2021. **332**: p. 127-147.
20. Hwang, D., J.D. Ramsey, and A.V. Kabanov, *Polymeric micelles for the delivery of poorly soluble drugs: from nanoformulation to clinical approval.* Advanced Drug Delivery Reviews, 2020. **156**: p. 80-118.
21. Hussein, Y.H. and M. Youssry, *Polymeric micelles of biodegradable diblock copolymers: enhanced encapsulation of hydrophobic drugs.* Materials, 2018. **11**(5): p. 688.
22. Noolandi, J. and K.M. Hong, *Theory of block copolymer micelles in solution.* Macromolecules, 1983. **16**(9): p. 1443-1448.
23. Cammas, S., et al., *Thermo-responsive polymer nanoparticles with a core-shell micelle structure as site-specific drug carriers.* Journal of Controlled Release, 1997. **48**(2-3): p. 157-164.

24. Lübtow, M.M., et al., *Ultra-high to ultra-low drug loaded micelles: Probing host-guest interactions by fluorescence spectroscopy.* Chemistry-A European Journal, 2019. **25**: p. 12601-12610.
25. Pöppler, A.C., et al., *Loading-Dependent Structural Model of Polymeric Micelles Encapsulating Curcumin by Solid-State NMR Spectroscopy.* Angewandte Chemie International Edition, 2019. **58**(51): p. 18540-18546.
26. Haider, M.S., et al., *Think beyond the core: The impact of the hydrophilic corona on the drug solubilization using polymer micelles.* ACS Applied Materials & Interfaces, 2020. **12**(22): p. 24531–24543.
27. Sochor, B., et al., *Probing the Complex Loading Dependent Structural Changes in Ultra-High Drug Loaded Polymer Micelles by Small-Angle Neutron Scattering.* Langmuir, 2020. **36**: p. 3494-3503.
28. Slor, G., et al., *Judging Enzyme-Responsive Micelles by Their Covers: Direct Comparison of Dendritic Amphiphiles with Different Hydrophilic Blocks.* Biomacromolecules, 2021. **22**(3): p. 1197–1210.
29. Cao, C., et al., *Drug-Induced Morphology Transition of Self-Assembled Glycopolymers: Insight into the Drug–Polymer Interaction.* Chemistry of Materials, 2018. **30**(15): p. 5227-5236.
30. Holder, S.J. and N.A. Sommerdijk, *New micellar morphologies from amphiphilic block copolymers: disks, toroids and bicontinuous micelles.* Polymer Chemistry, 2011. **2**(5): p. 1018-1028.
31. Schulz, A., et al., *Drug-induced morphology switch in drug delivery systems based on poly(2-oxazoline)s.* ACS Nano, 2014. **8**(3): p. 2686-2696.
32. Lim, C., et al., *Drug-dependent morphological transitions in spherical and worm-like polymeric micelles define stability and pharmacological performance of micellar drugs.* bioRxiv, 2021.
33. Nishiyama, N. and K. Kataoka, *Current state, achievements, and future prospects of polymeric micelles as nanocarriers for drug and gene delivery.* Pharmacology & Therapeutics, 2006. **112**(3): p. 630-648.
34. Cabral, H. and K. Kataoka, *Progress of drug-loaded polymeric micelles into clinical studies.* Journal of Controlled Release, 2014. **190**: p. 465-476.
35. Hwang, D., et al., *Poly(2-oxazoline) nanoparticle delivery enhances the therapeutic potential of vismodegib for medulloblastoma by improving CNS pharmacokinetics and reducing systemic toxicity.* Nanomedicine: Nanotechnology, Biology and Medicine, 2021. **32**: p. 102345.
36. Batrakova, E.V. and A.V. Kabanov, *Pluronic block copolymers: evolution of drug delivery concept from inert nanocarriers to biological response modifiers.* Journal of Controlled Release, 2008. **130**(2): p. 98-106.
37. Bloksma, M.M., U.S. Schubert, and R. Hoogenboom, *Poly(cyclic imino ether)s Beyond 2-Substituted-2-oxazolines.* Macromolecular Rapid Communications, 2011. **32**(18): p. 1419-1441.
38. Trachsel, L., M. Zenobi-Wong, and E.M. Benetti, *The role of poly(2-alkyl-2-oxazoline)s in hydrogels and biofabrication.* Biomaterials Science, 2021. **9**(8): p. 2874-2886.
39. You, Y., et al., *Engineered cell-degradable poly (2-alkyl-2-oxazoline) hydrogel for epicardial placement of mesenchymal stem cells for myocardial repair.* Biomaterials, 2021. **269**: p. 120356.
40. Trachsel, L., et al., *Double-network hydrogels including enzymatically crosslinked poly-(2-alkyl-2-oxazoline) s for 3D bioprinting of cartilage-engineering constructs.* Biomacromolecules, 2019. **20**(12): p. 4502-4511.
41. Luxenhofer, R., et al., *Poly(2-oxazoline)s as Polymer Therapeutics.* Macromolecular Rapid communications, 2012. **33**(19): p. 1613-1631.
42. He, Z., et al., *Poly(2-oxazoline) based micelles with high capacity for 3rd generation taxoids: Preparation, in vitro and in vivo evaluation.* Journal of Controlled Release, 2015. **208**: p. 67-75.

43. Lübtow, M.M., et al., *Drug induced micellization into ultra-high capacity and stable curcumin nanoformulations: Physico-chemical characterization and evaluation in 2D and 3D in vitro models.* Journal of Controlled Release, 2019. **303**: p. 162-180.
44. Haider, M.S., et al., *A Micellar Mitotane Formulation with High Drug-Loading and Solubility: Physico-Chemical Characterization and Cytotoxicity Studies in 2D and 3D In Vitro Tumor Models.* Macromolecular Bioscience, 2020. **20**(1): p. 1900178.
45. Vinod, N., et al., *High-capacity poly(2-oxazoline) formulation of TLR 7/8 agonist extends survival in a chemo-insensitive, metastatic model of lung adenocarcinoma.* Science Advances, 2020. **6**(25): p. 5542.
46. Hwang, D., et al., *Novel poly(2-oxazoline) block copolymer with aromatic heterocyclic side chains as a drug delivery platform.* Journal of Controlled Release, 2019. **307**: p. 261-271.
47. Park, J.-R., et al., *Influence of side-chain length on long-term release kinetics from poly(2-oxazoline)-drug conjugate networks.* European Polymer Journal, 2019. **120**: p. 109217.
48. Raveendran, R., et al., *Poly(2-oxazoline) block copolymer nanoparticles for curcumin loading and delivery to cancer cells.* European Polymer Journal, 2017. **93**: p. 682-694.
49. Lorson, T., et al., *Poly(2-oxazoline)s based biomaterials: A comprehensive and critical update.* Biomaterials, 2018. **178**: p. 204-280.
50. Zahoranová, A. and R. Luxenhofer, *Poly(2-oxazoline)- and Poly(2-oxazine)-Based Self-Assemblies, Polyplexes, and Drug Nanoformulations-An Update.* Advanced Healthcare Materials, 2021. **10**(6): p. 2001382.
51. Hu, C., et al., *A Thermogelling Organic-Inorganic Hybrid Hydrogel with Excellent Printability, Shape Fidelity and Cytocompatibility for 3D Bioprinting.* ChemRxiv, 2021.
52. Zhang, N., et al., *Cylindrical molecular brushes of poly (2-oxazoline) s from 2-isopropenyl-2-oxazoline.* Macromolecules, 2009. **42**(6): p. 2215-2221.
53. Lübtow, M.M., et al., *Like Dissolves Like? A Comprehensive Evaluation of Partial Solubility Parameters to Predict Polymer-Drug Compatibility in Ultra-High Drug Loaded Polymer Micelles.* Biomacromolecules, 2019. **20**(8): p. 3041-3056.
54. Sahn, M., C. Weber, and U.S. Schubert, *Poly(2-oxazoline)-Containing Triblock Copolymers: Synthesis and Applications.* Polymer Reviews, 2019. **59**(2): p. 240-279.
55. Zahoranová, A., et al., *ABA and BAB Triblock Copolymers Based on 2-Methyl-2-oxazoline and 2-n-Propyl-2-oxazoline: Synthesis and Thermoresponsive Behavior in Water.* Macromolecular Chemistry and Physics, 2017. **218**(13): p. 1700031.
56. Sedlacek, O. and R. Hoogenboom, *Drug Delivery Systems Based on Poly(2-Oxazoline)s and Poly(2-Oxazine)s.* Advanced Therapeutics, 2020. **3**(1): p. 1900168.
57. Hwang, D., et al., *Bioequivalence assessment of high-capacity polymeric micelle nanoformulation of paclitaxel and Abraxane® in rodent and non-human primate models using a stable isotope tracer assay.* Biomaterials, 2021: p. 121140.
58. He, Z., et al., *A high capacity polymeric micelle of paclitaxel: Implication of high dose drug therapy to safety and in vivo anti-cancer activity.* Biomaterials, 2016. **101**: p. 296-309.
59. Wan, X., et al., *Drug Combination Synergy in worm-like Polymeric Micelles Improves Treatment Outcome for Small Cell and Non-Small Cell Lung Cancer.* ACS Nano, 2018. **12**: p. 2426-2439.
60. Wan, X., et al., *Co-delivery of paclitaxel and cisplatin in poly (2-oxazoline) polymeric micelles: Implications for drug loading, release, pharmacokinetics and outcome of ovarian and breast cancer treatments.* Biomaterials, 2019. **192**: p. 1-14.
61. Witte, H. and W. Seeliger, *Cyclische imidsäureester aus nitrilen und aminoalkoholen.* Leibigs Ann., 1974. **1974**: p. 996-1009.
62. Lübtow, M.M., et al., *Drug specificity, synergy and antagonism in ultrahigh capacity poly(2-oxazoline)/poly(2-oxazine) based formulations.* Journal of the American Chemical Society, 2017. **139**(32): p. 10980-10983.

63. Hahn, L., et al., *Investigating the Influence of Aromatic Moieties on the Formulation of Hydrophobic Natural Products and Drugs in Poly(2-oxazoline)-Based Amphiphiles.* Biomacromolecules, 2018. **19**(7): p. 3119.
64. Lübtow, M.M., et al., *More Is Sometimes Less: Curcumin and Paclitaxel Formulations Using Poly(2-oxazoline) and Poly(2-oxazine)-Based Amphiphiles Bearing Linear and Branched C9 Side Chains.* Macromolecular Bioscience, 2018. **18**: p. 1800155-1800172.
65. Letchford, K., R. Liggins, and H. Burt, *Solubilization of hydrophobic drugs by methoxy poly(ethylene glycol)-block-polycaprolactone diblock copolymer micelles: Theoretical and experimental data and correlations.* Journal of Pharmaceutical Sciences, 2008. **97**(3): p. 1179-1190.
66. Fedors, R.F., *A method for estimating both the solubility parameters and molar volumes of liquids.* Polymer Engineering & Science, 1974. **14**(2): p. 147-154.
67. Van Krevelen, D.W. and K. Te Nijenhuis, *Properties of polymers: their correlation with chemical structure; their numerical estimation and prediction from additive group contributions*. 2009: Elsevier.
68. Mastronarde, D.N., *Automated electron microscope tomography using robust prediction of specimen movements.* Journal of structural biology, 2005. **152**(1): p. 36-51.
69. Luxenhofer, R., et al., *Doubly amphiphilic poly(2-oxazoline)s as high-capacity delivery systems for hydrophobic drugs.* Biomaterials, 2010. **31**: p. 4972-4979.
70. Han, Y., et al., *Synergistic combinations of multiple chemotherapeutic agents in high capacity poly(2-oxazoline) micelles.* Molecular Pharmaceutics, 2012. **9**(8): p. 2302-2313.
71. Seo, Y., et al., *Poly(2-oxazoline) block copolymer based formulations of taxanes: effect of copolymer and drug structure, concentration, and environmental factors.* Polymers for Advanced Technologies, 2015. **26**: p. 837-850.
72. Luxenhofer, R., et al., *Structure-property relationship in cytotoxicity and cell uptake of poly(2-oxazoline) amphiphiles.* Journal of Controlled Release, 2011. **153**(1): p. 73-82.
73. Liu, J., Y. Xiao, and C. Allen, *Polymer–drug compatibility: a guide to the development of delivery systems for the anticancer agent, ellipticine.* Journal of Pharmaceutical Sciences, 2004. **93**(1): p. 132-143.
74. Lin, S.-Y., C.-J. Lee, and Y.-Y. Lin, *Drug-polymer interaction affecting the mechanical properties, adhesion strength and release kinetics of piroxicam-loaded Eudragit E films plasticized with different plasticizers.* Journal of Controlled Release, 1995. **33**(3): p. 375-381.
75. Wu, C. and J.W. McGinity, *Non-traditional plasticization of polymeric films.* International Journal of Pharmaceutics, 1999. **177**(1): p. 15-27.
76. Nair, R., et al., *Influence of various drugs on the glass transition temperature of poly (vinylpyrrolidone): a thermodynamic and spectroscopic investigation.* International Journal of Pharmaceutics, 2001. **225**(1-2): p. 83-96.
77. Hossin, B., K. Rizi, and S. Murdan, *Application of Hansen Solubility Parameters to predict drug–nail interactions, which can assist the design of nail medicines.* European Journal of Pharmaceutics and Biopharmaceutics, 2016. **102**: p. 32-40.
78. Hansen, C.M., *Hansen solubility parameters: a user's handbook*. 2007: CRC press.
79. Barton, A.F., *CRC handbook of solubility parameters and other cohesion parameters*. 2017: Routledge.
80. Grüne, M., et al., *14 N–1 H HMQC solid-state NMR as a powerful tool to study amorphous formulations–an exemplary study of paclitaxel loaded polymer micelles.* Journal of Materials Chemistry B, 2020. **8**(31): p. 6827-6836.
81. Tian, Y., et al., *Designing micellar nanocarriers with improved drug loading and stability based on solubility parameter.* Molecular pharmaceutics, 2015. **12**(3): p. 816-825.
82. Raveendran, R., et al., *Poly (2-oxazoline) block copolymer nanoparticles for curcumin loading and delivery to cancer cells.* European Polymer Journal, 2017. **93**: p. 682-694.

83. Kim, Y., et al., *Effect of shell-crosslinking of micelles on endocytosis and exocytosis: acceleration of exocytosis by crosslinking.* Biomaterials Science, 2013. **1**(3): p. 265-275.
84. Dag, A., et al., *Modulating the cellular uptake of platinum drugs with glycopolymers.* Polymer Chemistry, 2016. **7**(5): p. 1031-1036.
85. Chang, T., et al., *Size effects of self-assembled block copolymer spherical micelles and vesicles on cellular uptake in human colon carcinoma cells.* Journal of Materials Chemistry B, 2014. **2**(19): p. 2883-2891.
86. Lübtow, M.M., et al., *In Vitro Blood–Brain Barrier Permeability and Cytotoxicity of an Atorvastatin-Loaded Nanoformulation Against Glioblastoma in 2D and 3D Models.* Molecular Pharmaceutics, 2020. **17**(6): p. 1835-1847.
87. Hiller, W., et al., *Micellization and mobility of amphiphilic poly (2-oxazoline) based block copolymers characterized by 1H NMR spectroscopy.* Macromolecules, 2015. **48**(12): p. 4032-4045.
88. Novakovic, D., et al., *Understanding dissolution and crystallization with imaging: A surface point of view.* Molecular Pharmaceutics, 2018. **15**(11): p. 5361-5373.
89. Hahn, L., et al., *Inverse thermogelation of aqueous triblock copolymer solutions into macroporous shear-thinning 3D printable inks.* ACS applied materials & interfaces, 2020. **12**(11): p. 12445-12456.
90. Lim, C., et al., *Drug-dependent morphological transitions in spherical and worm-like polymeric micelles define stability and pharmacological performance of micellar drugs.* bioRxiv, 2021.
91. Löscher, W. and H. Potschka, *Blood-brain barrier active efflux transporters: ATP-binding cassette gene family.* NeuroRx, 2005. **2**(1): p. 86-98.
92. Löscher, W., et al., *Drug resistance in epilepsy: clinical impact, potential mechanisms, and new innovative treatment options.* Pharmacological reviews, 2020. **72**(3): p. 606-638.
93. Neuwelt, E.A., et al., *Engaging neuroscience to advance translational research in brain barrier biology.* Nature Reviews Neuroscience, 2011. **12**(3): p. 169-182.
94. Hemmelmann, M., et al., *HPMA based amphiphilic copolymers mediate central nervous effects of domperidone.* Macromolecular rapid communications, 2011. **32**(9-10): p. 712-717.
95. Hemmelmann, M., et al., *Amphiphilic HPMA–LMA copolymers increase the transport of Rhodamine 123 across a BBB model without harming its barrier integrity.* Journal of controlled release, 2012. **163**(2): p. 170-177.
96. Clemens-Hemmelmann, M., et al., *Amphiphilic copolymers shuttle drugs across the blood–brain barrier.* Macromolecular bioscience, 2016. **16**(5): p. 655-665.
97. Demey, H., et al., *Propylene glycol-induced side effects during intravenous nitroglycerin therapy.* Intensive care medicine, 1988. **14**(3): p. 221-226.
98. Yaucher, N.E., et al., *Propylene glycol-associated renal toxicity from lorazepam infusion.* Pharmacotherapy: The Journal of Human Pharmacology and Drug Therapy, 2003. **23**(9): p. 1094-1099.

Supporting Information

Unlocking the Therapeutic Potential of RET agonist: Nanoformulations of BT44, *In vitro* and *In vivo* Evaluation for Treatment of Neurodegenerative Disorders.

Or

Unlocking the Therapeutic Potential of RET agonist: Nanoformulations of BT44, their biological activity *In vitro*, absorption, BBB penetration and toxicity.

Malik Salman Haider[1,‡], Arun K Mahato[2,‡], Anastasiia Kotliarova[2], Stefan Forster[1], Bettina Böttcher[3], Philipp Stahlhut[4], Yulia Sidorova[2,*], Robert Luxenhofer[1,5,*]

[1]*Functional Polymer Materials, Chair for Advanced Materials Synthesis, Institute for Functional Materials and Biofabrication, Department of Chemistry and Pharmacy, Julius-Maximilians-University Würzburg, Röntgenring 11, 97070 Würzburg, Germany*

[2]*Laboratory of Molecular Neuroscience, Institute of Biotechnology, HiLIFE, University of Helsinki, 00014, Helsinki, Finland*

[3]*Biocenter and Rudolf Virchow Centre, Julius-Maximilians-University Würzburg, Haus D15, Josef-Schneider-Str. 2, 97080 Würzburg, Germany*

[4]*Department of Functional Materials in Medicine and Dentistry, Institute of Functional Materials and Biofabrication and Bavarian Polymer Institute, Julius-Maximilians-University Würzburg, Pleicherwall 2, 97070 Würzburg, Germany*

[5]*Soft Matter Chemistry, Department of Chemistry, and Helsinki Institute of Sustainability Science, Faculty of Science, University of Helsinki, PB 55, 00014 Helsinki, Finland*

Synthesis 1: 2-*n*-pentyl-2-oxazoline Monomer

Hexanenitrile 17.55 g (180.58 mmol; 1.0 eq)

Ethanolamine 13.24 g (216.70 mmol; 1.20 eq)

$ZnAc_2.(H_2O)_2$	0.99 g	(4.51 mmol; 0.025 eq)
Boiling point	78°C (17 mbar)	
Yield	13.6 g (53 % of colourless liquid)	

Synthesis 2: A-pPentOx-A triblock copolymer

Inititation	MeOTf	0.539 g	(3.29 mmol; 1 eq)
1st block	MeOx	9.80 g	(115.2 mmol; 35 eq)
2nd block	PentOx	9.29 g	(65.81 mmol; 20 eq)
3rd block	MeOx	9.80 g	(115.2 mmol; 35 eq)
Termination	1 molar aqueous NaOH solution was added		
Solvent	Benzonitrile	65 ml	
Yield	26 g of white powder	92 %	
GPC (HFIP)	M_n = 3.4 kg/mol; Đ = 1.19		
^{1}H-NMR	M_n = 8.1 kg/mol		

DSC of three triblock copolymers

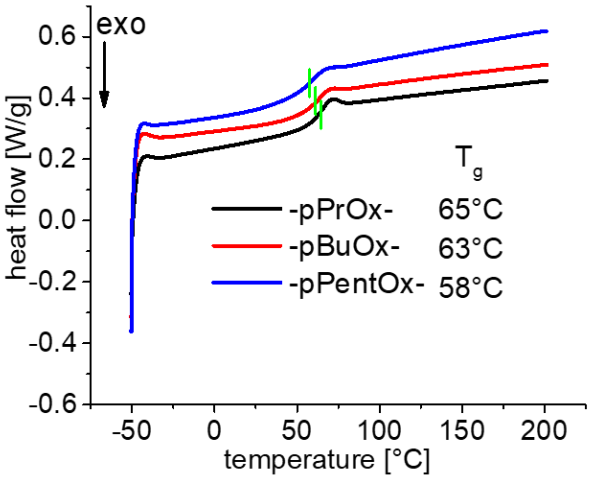

Figure S1: DSC thermogram of 3 triblock copolymer used in this study. The polymers are represented by their hydrophobic block only, while the hydrophilic block is always pMeOx in all the cases.Heat flow occurring during the second heating (10 K/min) cycle, green vertical line indicating the glass transition points.

Groups contributing towards the HSPs determination

Table S1: Groups contributing towards the calculation of Hansen solubility parameters by Hoftyzer and Van Krevelen's method according to the equation no. 4, 5 & 6 as given in the main text. The sulfone group was split into its components due to unavailability of data in the reference table [1].

Groups	pPrOx	pBuOx	pPentOx	pMeOx	BT44
CH_3-	1	1	1	1	1
-CH_2-	4	5	6	2	7
Phenyl	-	-	-	-	3
F	-	-	-	-	4
-O-	-	-	-	-	1
-CO-	1	1	1	1	1
>N-	1	1	1	1	3
SO_2 (-S/O-)	-	-	-	-	1/2
Ring	-	-	-	-	2

Quantification of BT44 by HPLC

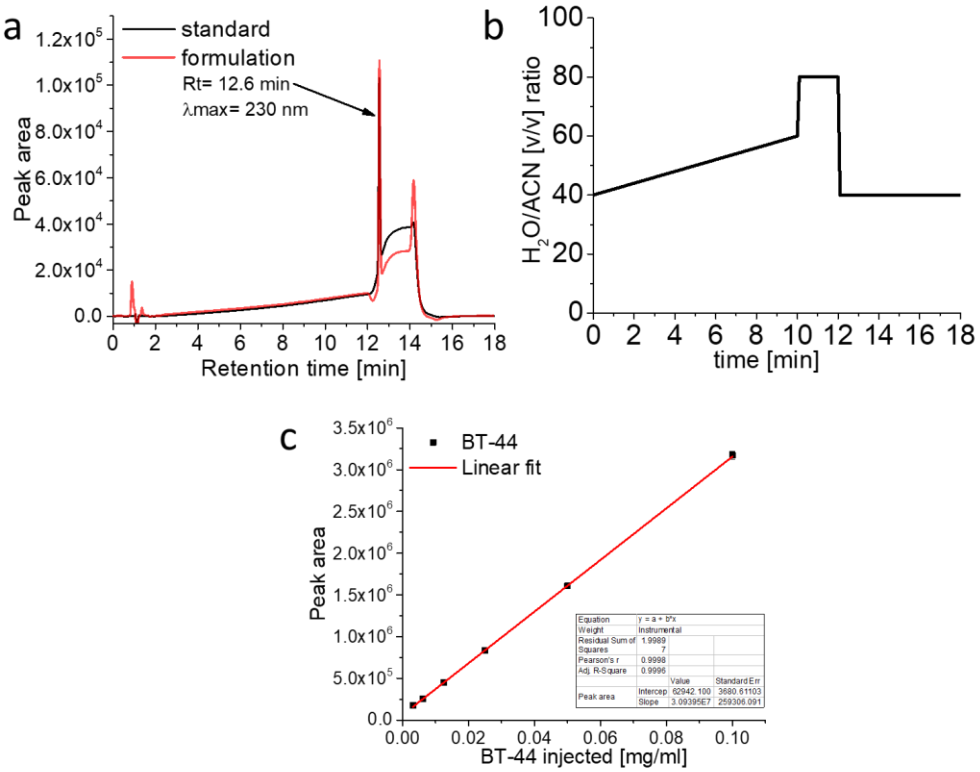

Figure S2: a) Normalized HPLC elugram of BT44, standard dilution (black) and formulation (red) at λ_{max} of 230 nm. Rt = 12.6 min. b) The HPLC method with the water/acetonitrile gradient (%) with the flow rate of 1ml/min. c) HPLC calibration curve of known amounts of BT44 injected and corresponding linear fit (red curve).

Visual appearance of the formulations

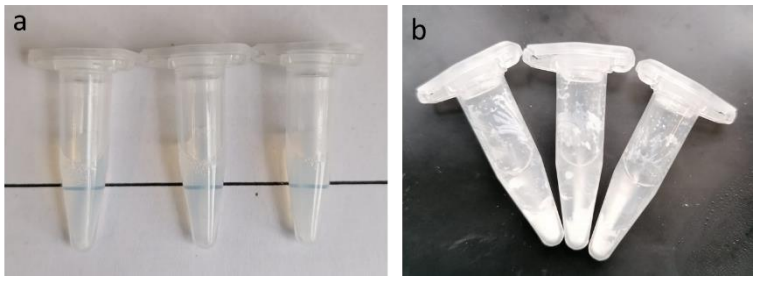

Figure S3: Visual appearance of the a) A-pPentOx-A/BT44 and b) A-pPrOx-A/BT44 formulation at 10/10 g/L polymer/BT44 feed (n=3).

^{1}H-NMR studies of the polymer and formulations

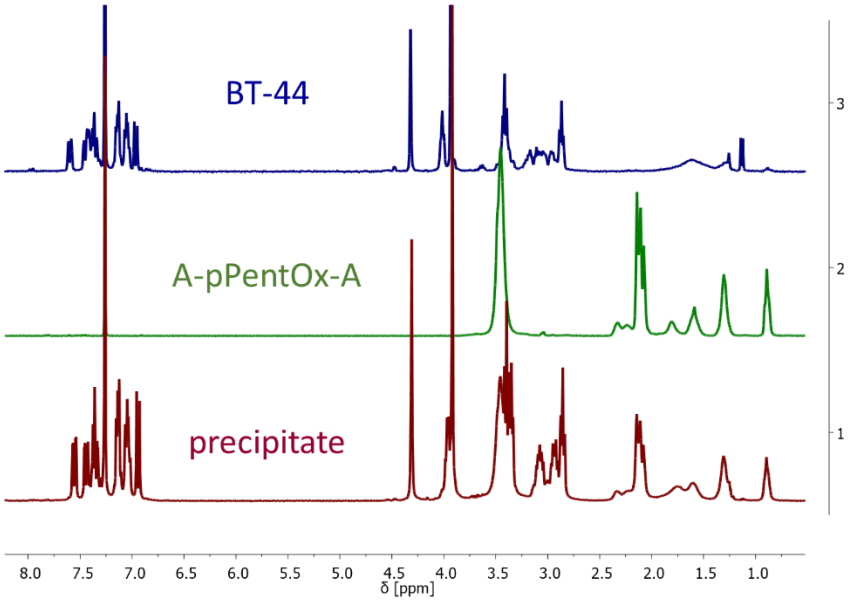

Figure S4: ^{1}H-NMR spectra (300 MHz, 298K) of the pure BT44 (blue), pure A-pPentOx-A polymer (green) and precipitate (red) formed during formulation development of A-pPentOx-A/BT44 (100/20 g/L). All the NMR spectra were collected in $CDCl_3$.

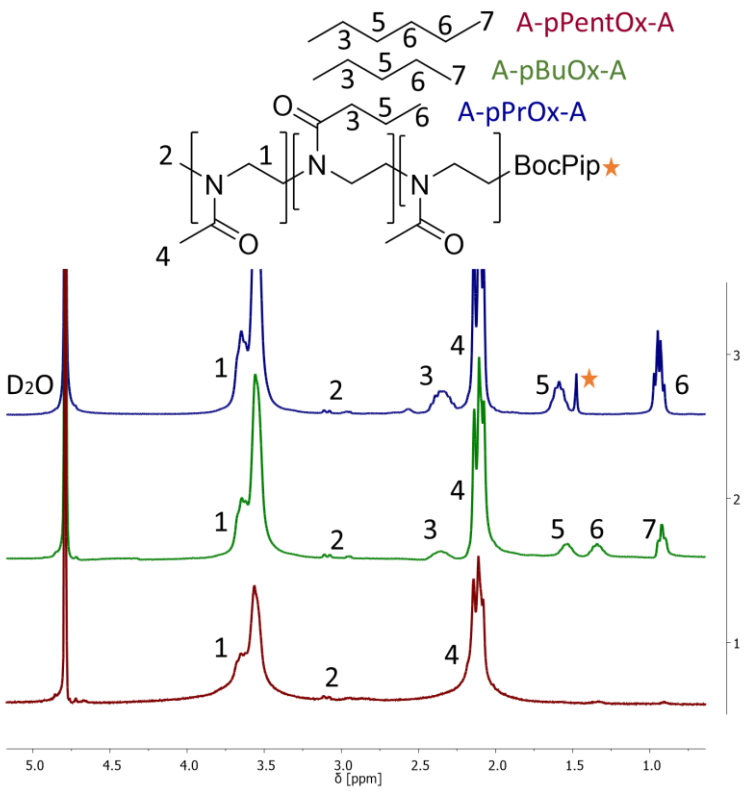

Figure S5: ^{1}H-NMR spectra (300 MHz, 298K) and chemical structures of the pure triblock copolymers i.e. A-pPrOx-A (blue), A-pBuOx-A (green) and A-pPentOx-A (red) in selective solvent D_2O at 10 g/L concentration with signal assignment of all major signals.

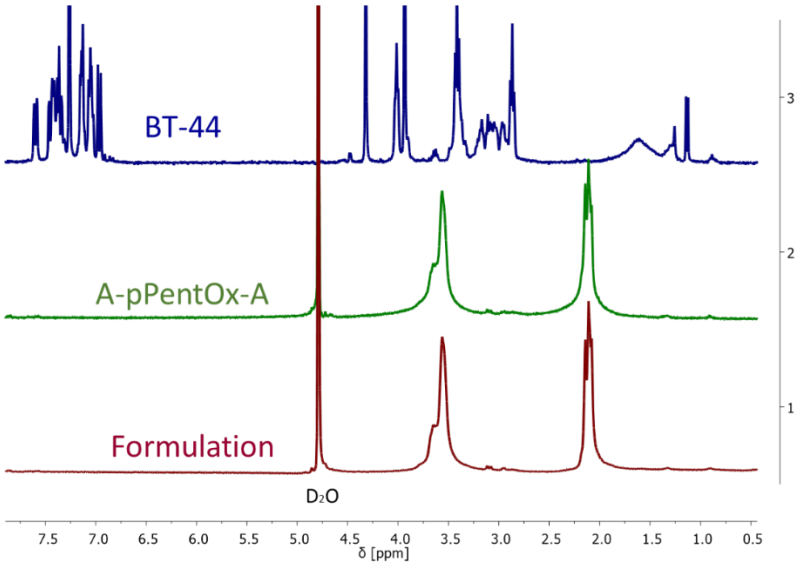

Figure S6: ^{1}H-NMR spectra (300 MHz, 298K) of the pure BT44 (blue) in $CDCl_3$, pure A-pPentOx-A polymer (green) and lyophilized formulation (A-pPentOx-A/BT44 100/20 g/L) collected in D_2O.

DSC studies of the formulations

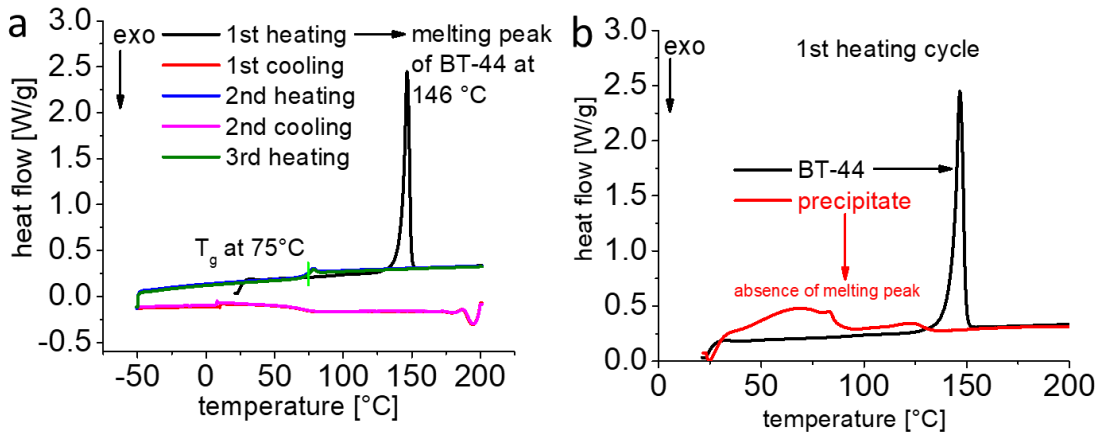

Figure S7: DSC thermogram of a) pristine BT44 with all the heating and cooling cycles (10 k/min). The sharp peak in first heating cycle at 146°C is the melting peak while the second and third heating cycles only exhibited the T_g (green vertical line at 75°C) and b) first heating cycle of pristine BT44 (black) and precipitated A-pPentOx-A/BT44 10/4 g/L formulation (red) at day 5 with sharp melting peak and absence of melting peak, respectively.

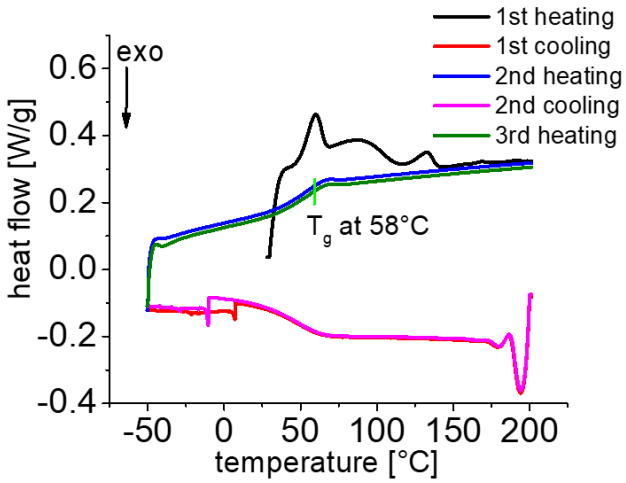

Figure S8: DSC thermogram with all the heating and cooling cycles (10 k/min) of A-pPentOx-A/BT44 100/20 g/L lyophilized formulation after 15 days of storage at room temperature. No melting peak of BT44 was to the T_g of A-pPentOx-A.

References SI:

1. Fedors, R.F., *A method for estimating both the solubility parameters and molar volumes of liquids.* Polymer Engineering & Science, 1974. **14**(2): p. 147-154.